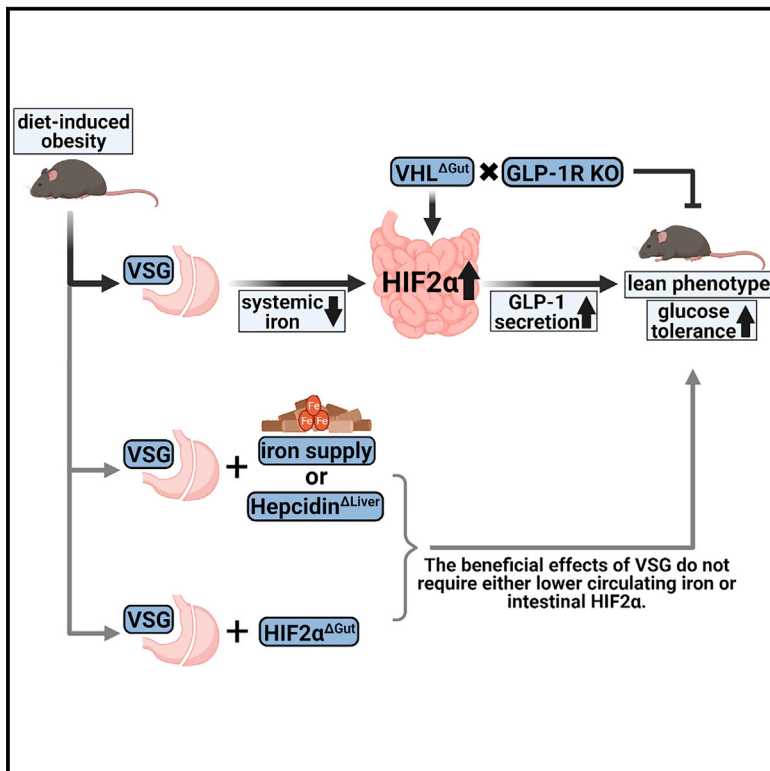


Gut HIF2 α signaling is increased after VSG, and gut activation of HIF2 α decreases weight, improves glucose, and increases GLP-1 secretion

Graphical abstract



Authors

Simon S. Evers, Yikai Shao, Sadeesh K. Ramakrishnan, ..., Darleen A. Sandoval, Yatrik M. Shah, Randy J. Seeley

Correspondence

seeleyrj@med.umich.edu

In brief

Bariatric surgery remains the most potent treatment for obesity and type 2 diabetes but also reduces iron levels. Evers et al. find that the machinery for absorbing iron is activated after VSG. Activation of this machinery recapitulates multiple effects of VSG. These findings may lead to less invasive therapies.

Highlights

- Bariatric surgeries result in reduced iron despite upregulation of absorption pathways
- Dietary or genetic manipulation to increase iron does not affect VSG effectiveness
- Genetic activation of intestinal HIF2 α results in improved body fat glucose tolerance
- Intestinal HIF2 α activation increases GLP-1 secretion, which mediates effects



Article

Gut HIF2 α signaling is increased after VSG, and gut activation of HIF2 α decreases weight, improves glucose, and increases GLP-1 secretion

Simon S. Evers,¹ Yikai Shao,¹ Sadeesh K. Ramakrishnan,² Jae Hoon Shin,¹ Nadejda Bozadjieva-Kramer,¹ Martin Irmiler,⁵ Kerstin Stemmer,^{6,7,8} Darleen A. Sandoval,^{1,4,9} Yatrik M. Shah,^{2,3} and Randy J. Seeley^{1,3,10,*}

¹Department of Surgery, University of Michigan, Ann Arbor, MI, USA

²Department of Molecular and Integrative Physiology, University of Michigan, Ann Arbor, MI, USA

³Department of Internal Medicine, University of Michigan, Ann Arbor, MI, USA

⁴Department of Nutrition, University of Michigan, Ann Arbor, MI, USA

⁵Institute of Experimental Genetics and German Mouse Clinic, Neuherberg, Germany

⁶Molecular Cell Biology, Institute for Theoretical Medicine, University of Augsburg, Augsburg, Germany

⁷Institute for Diabetes and Obesity, Helmholtz Zentrum München, Neuherberg, Germany

⁸German Center for Diabetes Research (DZD), Neuherberg, Germany

⁹Department of Pediatrics, Section of Nutrition, University of Colorado-Anschutz Medical Campus, Aurora, CO, USA

¹⁰Lead contact

*Correspondence: seeleyrj@med.umich.edu

<https://doi.org/10.1016/j.celrep.2021.110270>

SUMMARY

Gastric bypass and vertical sleeve gastrectomy (VSG) remain the most potent and durable treatments for obesity and type 2 diabetes but are also associated with iron deficiency. The transcription factor HIF2 α , which regulates iron absorption in the duodenum, increases following these surgeries. Increasing iron levels by means of dietary supplementation or hepatic hepcidin knockdown does not undermine the effects of VSG, indicating that metabolic improvements following VSG are not secondary to lower iron levels. Gut-specific deletion of *Vhl* results in increased constitutive duodenal HIF2 α signaling and produces a profound lean, glucose-tolerant phenotype that mimics key effects of VSG. Interestingly, intestinal *Vhl* deletion also results in increased intestinal secretion of GLP-1, which is essential for these metabolic benefits. These data demonstrate a role for increased duodenal HIF2 α signaling in regulating crosstalk between iron-regulatory systems and other aspects of systemic physiology important for metabolic regulation.

INTRODUCTION

Bariatric surgery remains the most effective treatment for obesity and type 2 diabetes (Cummings et al., 2016; Schauer et al., 2017; Mingrone et al., 2021). This includes procedures such as vertical sleeve gastrectomy (VSG), which is now the most common bariatric procedure (Welbourn et al., 2019). However, VSG is invasive and requires permanent anatomical alteration of the gastrointestinal (GI) tract. Consequently, surgical interventions cannot be scaled to provide relief for the large populations of individuals with obesity and/or type 2 diabetes. This emphasizes the need to understand how VSG and other bariatric procedures exert their potent beneficial effects at a mechanistic level.

Although physical restriction and malabsorption remain common explanations (le Roux and Bueter, 2014; Arble et al., 2018; Evers et al., 2019), a wide range of data points toward these being inadequate to account for the many physiological changes that occur after VSG (Stefater et al., 2010; Ryan et al., 2014). One important example is that VSG results in a weight-independent effect to profoundly increase post-prandial

secretion of gut hormones such as GLP-1 (Chambers et al., 2011). These changes emphasize the idea that critical for the effects of bariatric surgery are alterations in signals coming from the gut that affect a wide range of physiologies across many organ systems (Abu-Gazala et al., 2018; Ben-Zvi et al., 2018).

Use of bariatric surgery is not limited just by its invasiveness but by some long-term unwanted side effects, which include persistent hypoglycemia, acid reflux, and nutrient deficiencies. One of the most common nutrient deficiencies is a reduction in circulating iron and related increased rates of iron deficiency anemias (Ruz et al., 2009; Steenackers et al., 2018; Gowanlock et al., 2020; Mechanick et al., 2020). Iron regulation involves several organ systems, starting with the proximal portion of the small intestine. Iron absorption from the apical side of the intestine involves several enzymes and transporters whose expression is controlled by the transcription factor hypoxia-inducible factor (HIF) 2 α (Anderson et al., 2013; Shah and Xie, 2014). Low iron conditions increase HIF2 α signaling in the epithelium of the intestine. In turn, HIF2 α stimulates transcription of the apical iron transporters divalent metal transporter 1 (*Dmt1*) and



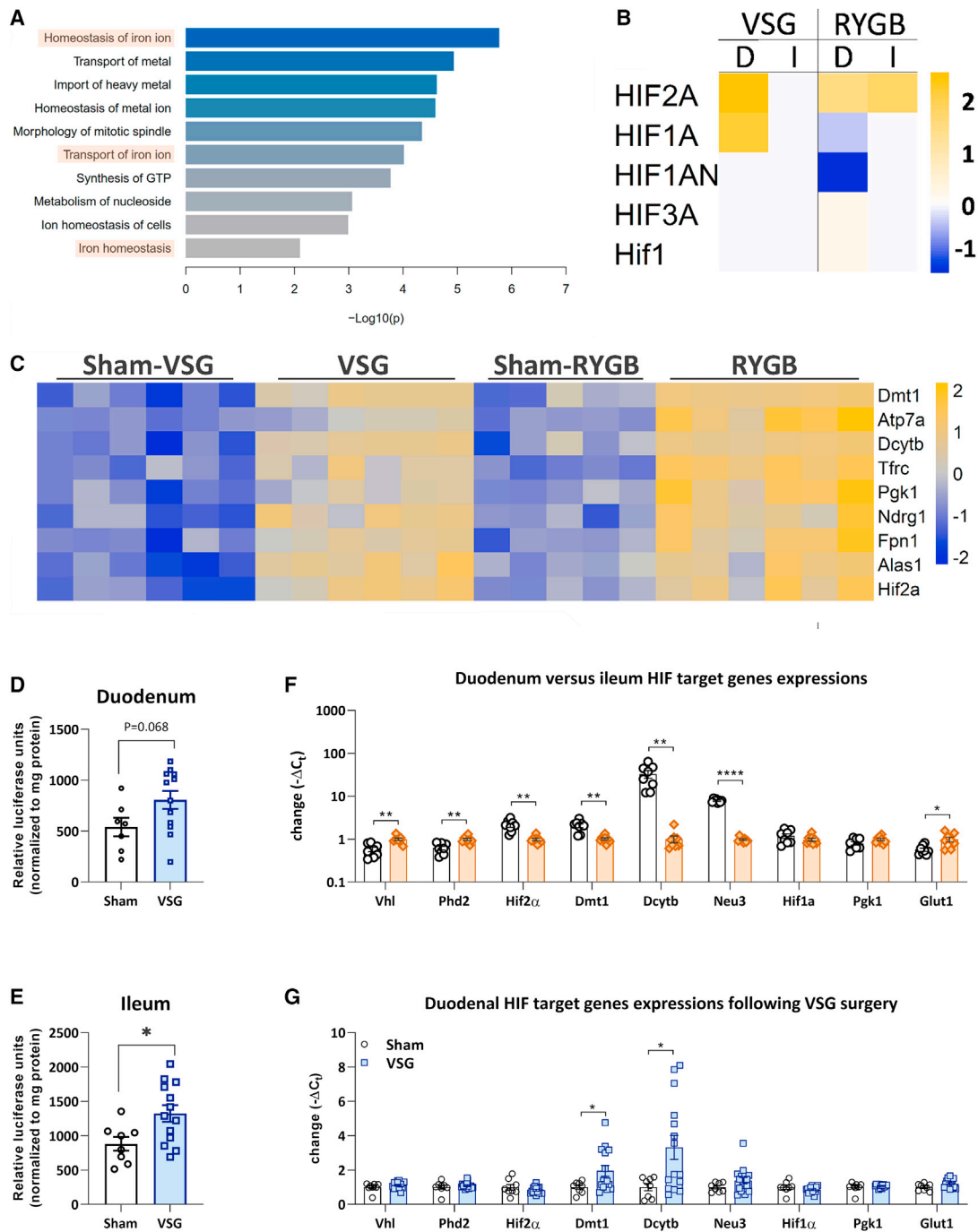


Figure 1. HIF2 α target genes are overexpressed specifically in the duodenum following bariatric surgery

(A) Unbiased enrichment analysis based on the “Function and Disease” category in Ingenuity Pathway Analysis (IPA) shows strong commonality in iron transport homeostatic pathway effects following both RYGB and VSG. These results are based on the overlap of 100 regulated genes in the duodenum upon RYGB and VSG treatment. Shown are $-\log_{10}(p)$ values.

(B) IPA upstream regulator analysis predicts activation of *Hif2 α* in the duodenum, D, following RYGB and VSG, based on increased downstream target gene expression levels. Note that *Hif2 α* activation is specific to the VSG duodenum and not the ileum, I.

(C) Heatmap of selected significantly regulated genes related to iron absorption (false discovery rate [FDR] < 10%) in the duodenum upon VSG and RYGB treatments compared with sham-operated rats. Shown are Z scores indicating significant activation (Z score > 2) or inhibition (Z score < -2).

(D and E) In ODD-luciferase mice, luciferase expression is increased in the (D) duodenum and (E) ileum, indicative of increased HIF1/2 α protein activity. Average \pm SEM; sham, n = 7/8; VSG, n = 12/13; *p < 0.05, unpaired t test.

(legend continued on next page)

duodenal cytochrome *b* (*Dcytb*), which facilitate transport of iron from the chyme into intestinal cells.

HIF2 α also stimulates expression of the basolateral iron transporter ferroportin to transport iron from intestinal cells into the circulation (Lane et al., 2015). Because iron is not only an essential micronutrient but also toxic at higher concentrations, circulating iron levels are tightly regulated. Iron entering the circulation from the basolateral side of the intestine can be inhibited by the hepatic hormone hepcidin (Ganz and Nemeth, 2012). Increased circulating iron levels stimulate hepcidin, which blocks the ferroportin transporter and inhibits iron entering the circulation. Increased iron levels, in turn, reduce expression of HIF2 α , and, consequently, iron absorption from the chyme reduces (Mastrogiannaki et al., 2009; Taylor et al., 2011).

Intracellular HIF α expression (HIF1 α and HIF2 α) is regulated through prolyl hydroxylase (PHD) and the von Hippel-Lindau (VHL) proteins. Under sufficient oxygen conditions, HIFs are hydrolyzed by PHD and ubiquitinated by VHL, which sets them up for proteasomal degradation, preventing HIFs from going to the nucleus and influencing gene transcription (Ramakrishnan and Shah, 2017; Lee et al., 2020). Under insufficient oxygen conditions or hypoxia, HIF α binds to HIF β and, in the nucleus, forms a complex with Creb binding protein (CBP)/P300 that induces target gene transcription (Lando et al., 2002; Lee et al., 2020). The key point is that iron levels are regulated at multiple levels, including absorption in the gut, so that this necessary but toxic nutrient remains at appropriate levels.

It is commonly believed that bariatric surgery results in reduced iron levels because of less exposure of the duodenum to ingested food (Kotkiewicz et al., 2015). However, lower iron levels are also observed in surgeries with widely varying effects on duodenal exposure to chyme. Moreover, lowered iron levels can also be observed in well-controlled rodent models of disparate procedures (Arble et al., 2018). Because iron deficiency and related anemia are commonly observed following bariatric surgery, iron supplementation is recommended as part of post-operative care (Aarts et al., 2011; Mechanick et al., 2020). Nonetheless, apparent beneficial effects of iron supplementation seem to be limited as a successful strategy to reduce iron deficiency and are related to the type of iron supplemented (Mischler et al., 2018). This suggests that bariatric surgery specifically affects iron homeostasis at a mechanistic level.

We report here that, in the mouse and rat, transcriptional changes point toward an increase in HIF2 α signaling in the duodenum following bariatric surgery. This leads to the hypothesis, tested here, that VSG's ability to alter the iron-regulatory system also contributes to beneficial effects on body weight, glucose regulation, and gut hormone secretion and identifies HIF2 α -related signaling in the gut as an important regulator of systemic metabolism, body weight, and hormone secretion.

RESULTS

Bariatric surgery in rodents results in increased duodenal HIF2 α target gene expression

We first performed an unbiased transcriptomics analysis, comparing the duodenum of rats receiving VSG or Roux-en-Y Gastric Bypass (RYGB) surgery (see *in vivo* data from this cohort in Figure S1). Despite the profound differences in the functional effect on the duodenum between these two surgeries, there is an unbiased common response to upregulate HIF2 α and its target genes (Figures 1A–1C). To further determine whether HIF is upregulated following VSG, we performed VSG in a cohort of oxygen-dependent domain (ODD)-luciferase mice. These mice express luciferase at the ODD of HIF α and can therefore be used as a measure of HIF α activation. In this cohort, we found that luciferase activity, and therefore HIF α expression, was upregulated in the duodenum and ileum of mice with VSG (Figure 1D). However, luciferase activity at the ODD does not discriminate between HIF1 α or HIF2 α expression. We therefore compared the expression levels of both genes in the upper and lower small intestine (Figure 1E). This comparison showed that, in the proximal part of the small intestine, the duodenum, *Hif2 α* and its protein target genes *Dmt1*, *Dcytb*, and *Neu3*, are more highly expressed, whereas, in the distal part of the small intestine, the ileum, expression levels of *Vhl* and *Phd2* as well as the HIF1 α target gene *Glut1* are higher. In a separate cohort of mice (Figure 1F), we found that expression of HIF2 α target genes following VSG surgery was also upregulated in the duodenum, specifically of genes transcribing the iron transporters *Dmt1* ($p < 0.05$) and *Dcytb* ($p < 0.0001$). In contrast, the HIF1 α target genes *Pgk1* and *Glut1* were not upregulated.

Dietary iron supplementation or genetic manipulation to increase circulating iron does not alter the effectiveness of VSG to reduce body weight or glycemia

Unlike in most rodent experiments, humans are told to take considerable iron supplements after bariatric surgery to reduce potential anemias. If HIF2 α is a component of the surgical response, then higher iron levels could suppress HIF2 α signaling and may therefore undermine the effectiveness of the procedure. Hence, to increase circulating iron levels, we tested B6C57/j mice supplemented with a high-fat/high-iron (350 ppm) diet and mice with deletion of hepcidin in the liver (Hepcidin^{Δliver}). In both cases, VSG showed clear benefits to glucose regulation and body weight (Figure S2). In the case of dietary iron supplementation, no effect of supplementation on hematocrit was observed (Figure 2A), whereas a trend toward restored iron levels was observed (Figure 2B). Surprisingly, circulating hepcidin levels were increased in VSG mice fed a high-iron diet (Figure 2C). Likewise, Hepcidin^{Δliver} did

(F) mRNA expression analyses comparing epithelium of the duodenum and ileum from sham-operated mice, showing relatively higher expression levels for *Hif2 α* and its target genes *Dmt1*, *Dcytb*, and *Neu3* in the duodenum than the ileum. Average \pm SEM; duodenum, $n = 17$; ileum, $n = 17$; * $p < 0.05$, ** $p < 0.01$, **** $p < 0.0001$, multiple t test with Holm-Sidak correction.

(G) mRNA expression analyses of duodenal epithelium from mice following VSG confirmed increased expression levels for the HIF2 α target genes *Dmt1* and *Dcytb*. Average \pm SEM; sham, $n = 8$; VSG, $n = 15/16$; * $p < 0.05$; multiple t test with Holm-Sidak correction. Average Ct data of gene expression is available in Tables S1 and S2.

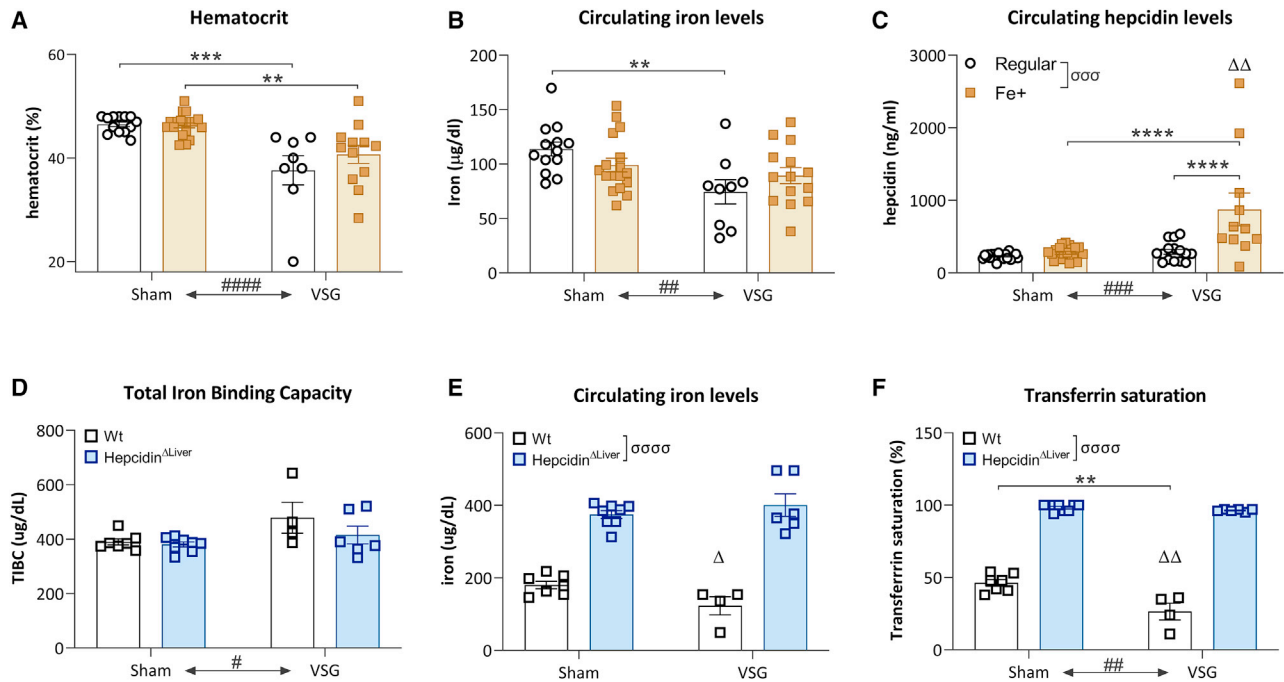


Figure 2. High dietary iron supplementation does not affect circulating iron following VSG

(A) VSG induced a reduction in hematocrit levels that could not be countered by high dietary iron levels. Average \pm SEM; sham-regular, n = 13; sham-Fe+, n = 20; VSG-regular, n = 8; VSG-Fe+, n = 12; two-way ANOVA, main effect ##### $p < 0.0001$ surgery effect, multiple comparisons post hoc Tukey test, ** $p < 0.01$, *** $p < 0.001$.

(B) VSG induced a reduction in circulating iron levels that could not be countered by high dietary iron levels. Two-way ANOVA, main effect ## $p < 0.01$ surgery effect, multiple comparisons post hoc Tukey test, ** $p < 0.01$.

(C) Circulating hepcidin levels were mostly increased in mice with VSG on a high-iron diet. Two-way ANOVA, main effects $\sigma\sigma\sigma p < 0.001$: dietary iron effect, ## $p < 0.001$: surgery effect, $\Delta\Delta p < 0.01$: interaction dietary iron*surgery; multiple comparisons post hoc Tukey test, **** $p < 0.0001$.

(D) VSG surgery, but not Hepcidin^{ΔLiver}, increased total iron binding capacity (TIBC). Average \pm SEM; sham-WT, n = 7; VSG-WT, n = 4; sham-Hepcidin^{ΔLiver}, n = 8; VSG-Hepcidin^{ΔLiver}, n = 6; # $p < 0.05$, two-way ANOVA, main effect of surgery.

(E) Hepcidin^{ΔLiver} increased circulating iron levels independent of surgery, although an interaction of lower iron levels in WT VSG was observed. $\Delta p < 0.05$: two-way ANOVA, interaction of genotype*surgery.

(F) At the level of transferrin saturation, a main effect of Hepcidin^{ΔLiver}, VSG surgery, and an interaction of genotype*surgery were observed. Two-way ANOVA, **** $p < 0.0001$: main effect of genotype, ## $p < 0.001$: main effect of surgery, $\Delta\Delta p < 0.01$: interaction genotype*surgery.

not alter the effect of VSG to increase total iron binding capacity (Figure 2D), and VSG did not lower circulating iron levels in the Hepcidin^{ΔLiver} (Figure 2E) or transferrin saturation (Figure 2F). These data indicate that the benefits of surgery are not secondary to lowering iron levels. Additionally, these data do not support use of VSG as a therapeutic option to treat high-iron conditions such as hemochromatosis. Moreover, these results suggest that intestinal iron transport into the circulation is actively suppressed even in the presence of lower hematocrit and circulating iron levels. Consequently, it appears that VSG surgery results in broad physiological changes that predispose the organism to maintaining lower circulating iron levels. The inability to reduce iron levels in hepcidin knockout (KO) mice points toward hepcidin being an important component of the effect of VSG to lower iron, but further work is warranted to fully identify the mechanisms by which VSG regulates hepcidin secretion and lowers iron levels.

Intestinal *Hif2 α* is not essential for the metabolic effects of VSG

Circulating iron levels do not seem to affect the metabolic consequences of VSG. We tested whether intestinal *Hif2 α* is essential for the effects of VSG. To do this, we developed a mouse with conditional KO of *Hif2 α* (*Hif2 α* ^{ΔGut}) in *Villin*^{CreERT}-expressing intestinal epithelial cells using tamoxifen administration 14 days prior to surgery. To confirm that *Hif2 α* was conditionally knocked out over the duration of the study, we measured mucosal duodenal *Hif2 α* (Figure 3A) and *Cre* (Figure 3B) mRNA expression and found that, after 84 days of induction, *Cre* was still highly expressed, whereas *Hif2 α* mRNA was decreased significantly in *Hif2 α* ^{ΔGut} mice. We found that *Hif2 α* ^{ΔGut} animals respond to VSG surgery in a similar fashion as their *Hif2 α* ^{F/F} wild-type (WT) littermates in terms of body weight (Figure 3C). Furthermore, following an intraperitoneal (i.p.; 2 g/kg glucose) or oral nutrient (2 g/kg glucose in Ensure Plus formula) challenge, we did not observe an effect of intestinal *Hif2 α* deletion on glucose response (Figure 3D) or post-prandial total GLP-1 levels (Figure 3E). Even though *Hif2 α* ^{ΔGut} did not affect food intake compared with WT littermates (Figure 3F), it did result in lower hepatic triglyceride levels compared with the WT, which was

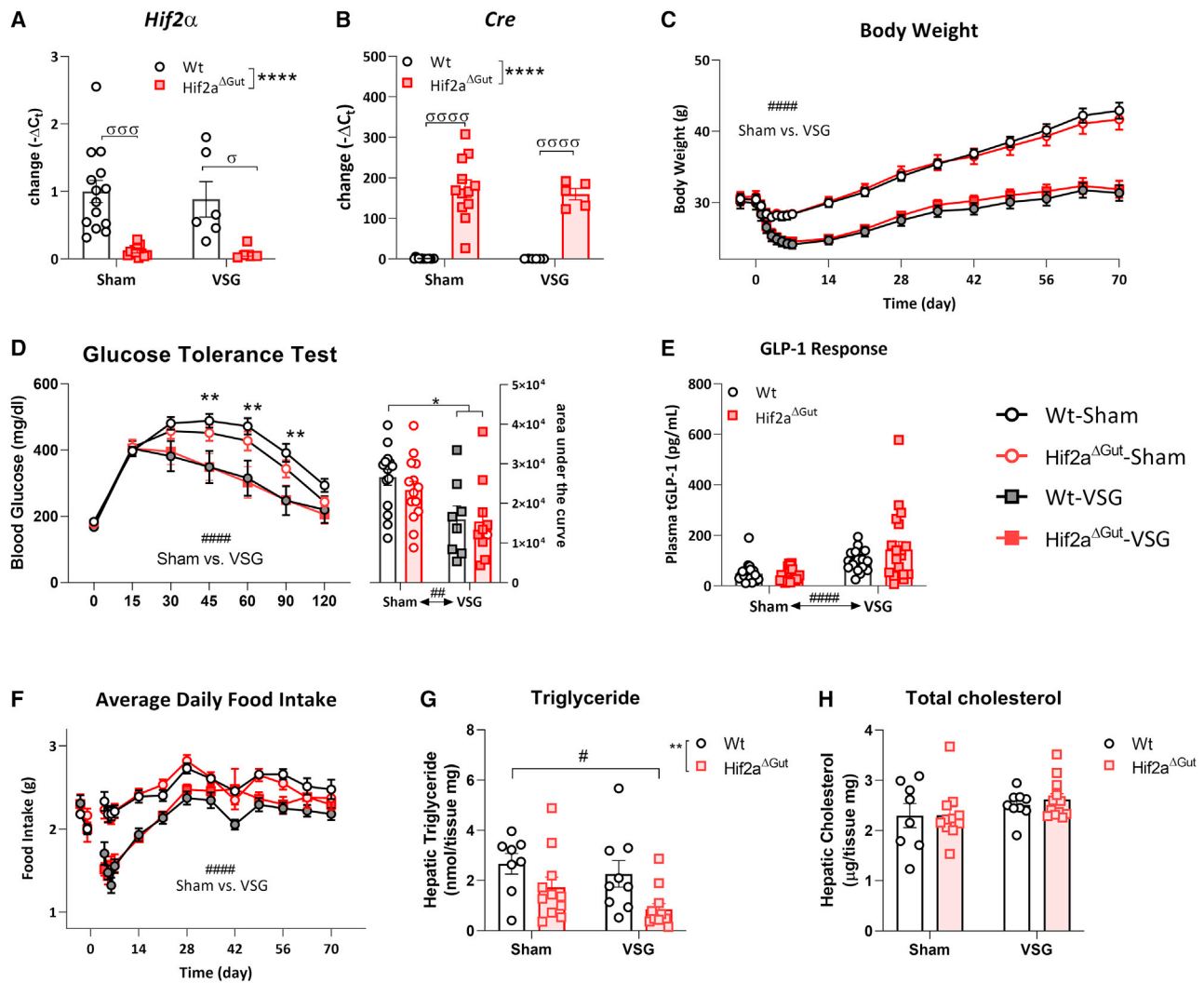


Figure 3. *Hif2α*^{ΔGut} does not affect the response to VSG surgery

(A) At termination, *Hif2α* is effectively knocked down in duodenal mucosal samples from *Cre*-expressing mice. Average \pm SEM; WT-sham, n = 25; WT-VSG, n = 18; *Hif2α*^{ΔGut}-sham, n = 25; *Hif2α*^{ΔGut}-VSG, n = 20. Two-way ANOVA: $F_{1,33} = 25.56$, ****p < 0.001.

(B) At termination, *Cre* is expressed in the duodenum of *Hif2α*^{Vf/Villin}*CreERT* (*Hif2α*^{ΔGut}) mice 84 days after tamoxifen *Cre* induction independent of surgery. Two-way ANOVA: $F_{1,33} = 105.6$, ****p < 0.001. Average Ct data are available in Table S3.

(C) Following VSG, mice follow a similar BW trajectory independent of genotype. rm-ANOVA: $F_{51,1638} = 4.851$, ####p < 0.0001 post hoc Tukey test.

(D) Glucose levels following i.p. glucose administration (2 g/kg glucose) are lowered after VSG compared with sham surgery independent of genotype. rm-ANOVA: $F_{18,301} = 1.575$, ####p < 0.0001 post hoc Tukey test, multiple comparisons **p < 0.05. The glucose area under the curve is lowered in VSG mice. Two-way ANOVA: $F_{1,43} = 0.2606$, ##p < 0.01 surgery effect, *p < 0.05 post hoc Tukey test.

(E) Total GLP-1 response 15 min after oral nutrient exposure (2 g/kg glucose in Ensure Plus) was increased after VSG; two-way ANOVA: $F_{1,84} = 2.619$, ####p < 0.0001, but not dependent on genotype.

(F) Food intake is reduced following VSG compared with sham surgery independent of genotype. rm-ANOVA: $F_{42,1250} = 2.826$, ####p < 0.0001 post hoc Tukey test.

(G) Hepatic triglyceride levels were lower in *Hif2α*^{ΔGut} mice. Average \pm SEM; WT-sham, n = 8; WT-VSG, n = 9; *Hif2α*^{ΔGut}-sham, n = 11; *Hif2α*^{ΔGut}-VSG, n = 12. Two-way ANOVA: $F_{1,36} = 8.891$, **p < 0.01 main effect *Hif2α*^{ΔGut}, #p < 0.05 post hoc Tukey test.

(H) No effects of surgery or genotype on hepatic total cholesterol levels were observed.

independent of surgical treatment (Figure 3G). No effects of either surgery or genotype were observed on hepatic total cholesterol levels (Figure 3H). These data reveal that, although intestinal *Hif2α*^{ΔGut} lowers liver triglyceride levels, intestinal *Hif2α* is not essential for the beneficial metabolic effects

observed following VSG. A possibility is that other HIFs may compensate for the lack of cellular HIF2α (Xie et al., 2017). For example, in this cohort under *ad libitum* feeding conditions, we found an increase in duodenal *Hif1α* expression between sham-operated mice (Figure S3). However, similar to previous

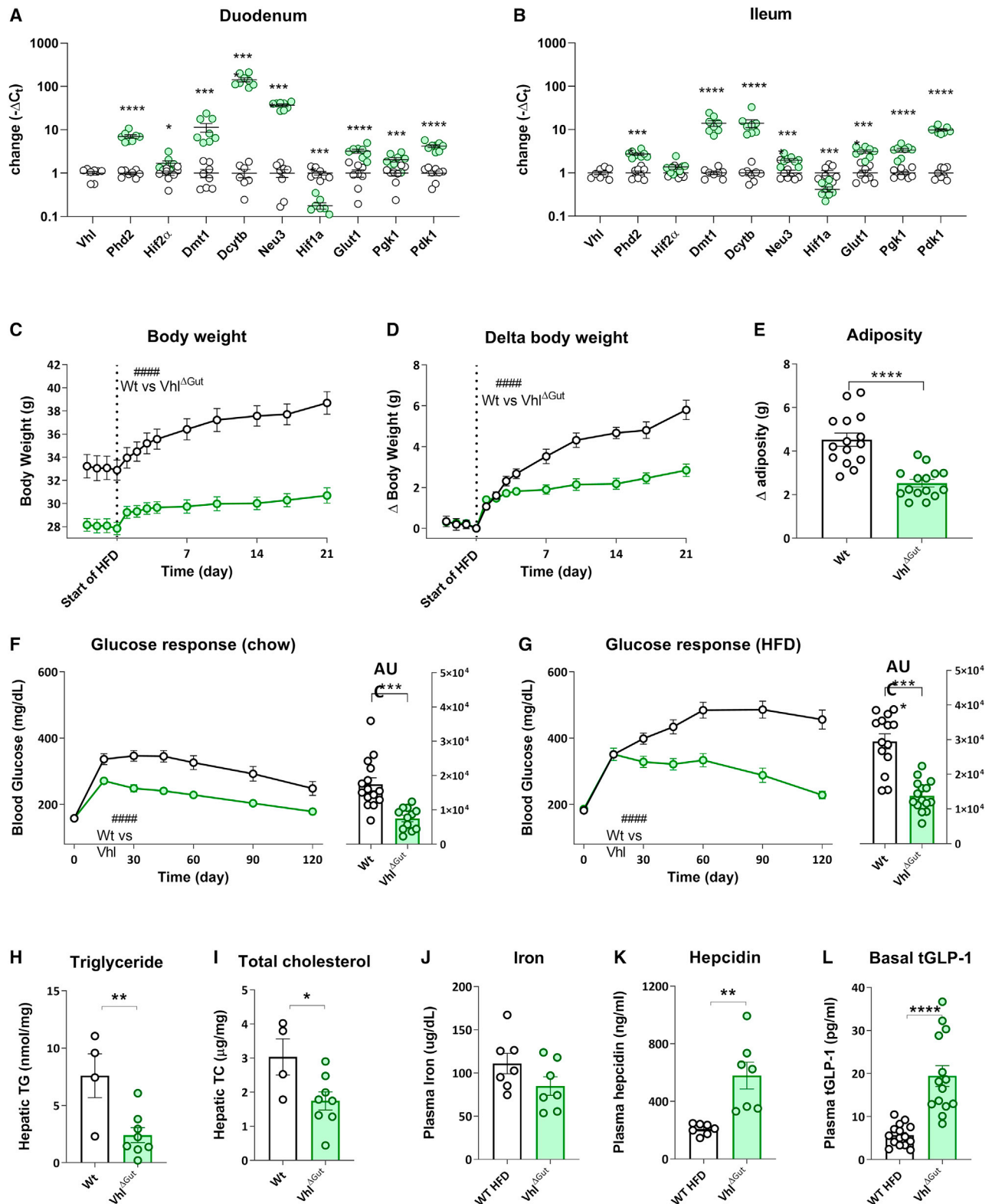


Figure 4. Intestinal *Vhl* deletion (*Vhl* Δ Gut)

(A and B) In the duodenum (A) and ileum (B), *Vhl* Δ Gut results in increased expression of the HIF2 α target genes *DMT1*, *Dcytb*, and *Neu3* and increased levels of the HIF1 α target genes *Glut1*, *Pgk1*, and *Pdk1*. Additionally, expression of *Phd2* is upregulated in the duodenum and ileum. Although *Hif2 α* gene expression is

(legend continued on next page)

observations by others (Das et al., 2019), knockdown of *Hif2α*^{ΔGut} did not result in a reduction of expression of the iron-related target genes *Dmt1* and *Dcytb*. Nonetheless, the HIF2α target gene *Neu3*, which has been shown to be under strict regulation of HIF2α (Xie et al., 2017), was downregulated (Figure S3).

Vhl^{ΔGut} results in increased HIF2α target gene expressions and a lean diet-induced obesity (DIO)-resistant and glucose-tolerant phenotype with increased circulating hepcidin and basal GLP-1 levels

Although we found that the lack of intestinal *Hif2α* did not affect the benefits of VSG surgery, we sought to identify the systemic effects of increased HIF and its target genes in the intestine. Therefore, we used another Cre-LoxP mouse model to delete *Vhl* in intestinal epithelial cells expressing Villin^{Cre} (*Vhl*^{ΔGut}). As expected, the mRNA levels of HIF1α target genes (*Glut1*, *Pdk1*, and *Pgk1*) and HIF2α target genes (*Dmt1*, *Dcytb*, and *Neu3*) were increased in the duodenum (Figure 4A) and ileum (Figure 4B) of *Vhl*^{ΔGut} mice. Although the potent increase in target gene expression indicates an increase in HIF1α and HIF2α activity at the protein level, the increase in Phd2 (PHD domain 2) gene expression suggests a feedback mechanism to downregulate HIF protein levels in *Vhl*^{ΔGut} mice. Interestingly, although *Hif1α* gene expression is reduced in both parts of the small intestine in *Vhl*^{ΔGut} mice, expression of *Hif2α* is unaffected in the ileum and even increased in the duodenum, suggesting negative feedback on *Hif1α* expression that is not present for *Hif2α* expression.

Strikingly, *Vhl*^{ΔGut} mice are lower in body weight compared with littermate controls when fed a standard chow diet (Figure 4C). Furthermore, when fed a 60% high-fat diet (HFD), *Vhl*^{ΔGut} mice showed profound resistance to DIO by gaining considerably less weight (Figures 4C and 4D) and adipose tissue mass (Figure 4E). Under chow-fed (Figure 4F) and HFD-fed (Figure 4G) conditions, *Vhl*^{ΔGut} mice had an improved glucose response during an ipGTT (2 g/kg glucose), suggesting improved glucose tolerance compared with WT mice. Furthermore, *Vhl*^{ΔGut} mice on an HFD had lower hepatic triglyceride (Figure 4H) and total cholesterol (Figure 4I) levels. Even though expression of iron transporter genes is increased in the intestine of *Vhl*^{ΔGut} mice, circulating iron levels were not different compared with littermate controls (Figure 4J). Similar to VSG, normal iron levels

are likely the result of an increase in circulating hepcidin levels preventing excessive iron from entering the circulation (Figure 4K). Interestingly, we found that, following 4 h of fasting, *Vhl*^{ΔGut} mice have higher circulating levels of total GLP-1 at baseline compared with WT littermates (Figure 4L).

Increased GLP-1 in *Vhl*^{ΔGut} mice originates from the intestine and is essential for its glucose-tolerant phenotype

We showed that intestinal *Hif2α* is not essential to induce an increased GLP-1 response following VSG and that *Vhl*^{ΔGut} mice have increased basal circulating GLP-1 levels. To examine the importance of increased basal total GLP-1 levels on the profound metabolic phenotype of the *Vhl*^{ΔGut}, we first determined the origin of the increased GLP-1; i.e., whether it comes from the intestine or pancreas. To do so, we bred *Vhl*^{IF/F}*Villin*^{Cre} (*Vhl*^{ΔGut}) with preproglucagon (*Gcg*)^{stopfloX} mice. This resulted in mice that do not express VHL in the intestine and are total *Gcg* body KO mice except for the intestine, in which *Gcg* is reactivated (RA). Because these mice only express *Gcg* in the intestine, any circulating GLP-1 is limited to what is secreted from villin-expressing cells in the intestine. We found that circulating GLP-1 levels are indeed increased similarly in *Vhl*^{ΔGut} mice and *Vhl*^{ΔGut}*_GcgRA*^{ΔGut} mice (Figure 5A), confirming that the intestine is the source of increased circulating GLP-1. Similarly, *GcGRA* mice have similar circulating levels of GLP-1 as littermate controls, suggesting that any circulating GLP-1 is secreted primarily from the intestine. To further confirm that circulating GLP-1 levels in these mice originate from the intestine, we measured pancreatic GLP-1 levels and indeed found that intestinal *GcgRA* resulted in limited to non-measurable pancreatic GLP-1 levels (Figure 5B).

Because the *Gcg*^{stopfloX} lacks glucagon as well, assessing improvements in their glucose regulation is not informative. Hence, to study whether the increased basal total GLP-1 levels observed in the *Vhl*^{ΔGut} mice is necessary for the lean and glucose-tolerant phenotype, we bred *Vhl*^{ΔGut} with GLP1 receptor stop-flox mice (*Glp1r*^{stopfloX}). This resulted in mice that are total body GLP1R KO mice except for Villin^{Cre}-expressing cells. However, because others have shown that GLP1R is not expressed in intestinal cells (Richards et al., 2014), we consider these mice to functionally be complete body *Glp1r* KO mice as well as intestine-specific VHL KO mice. *Vhl*^{ΔGut} and *Vhl*^{ΔGut}*Glp1r*^{KO}

upregulated in the duodenum, it is not affected in the ileum of *Vhl*^{ΔGut} mice. In contrast, *Hif1α* gene expression is downregulated in the duodenum and ileum of *Vhl*^{ΔGut} mice. Average ± SEM; WT, n = 8; *Vhl*^{ΔGut}, n = 8; multiple comparisons Holm-Sidak: *p < 0.05, ***p < 0.001, ****p < 0.0001. Average Ct data are available in Tables S5 and S6.

- (C) *Vhl*^{ΔGut} results in mice that are lower in body weight on chow as well as a 60% HFD; day 0–21; average ± SEM; WT, n = 15; *Vhl*^{ΔGut}, n = 15; rm-ANOVA: F_{12, 336} = 18.54, ####p < 0.0001.
(D) *Vhl*^{ΔGut} mice gain less weight and are DIO resistant to a 60% HFD; rm-ANOVA: F_{12, 336} = 18.30, ####p < 0.0001.
(E) *Vhl*^{ΔGut} mice gain less adipose mass when fed a 60% HFD; t test: t₂₈ = 5.763, ****p < 0.01.
(F) During an ipGTT (2 g/kg glucose), chow-fed *Vhl*^{ΔGut} mice have reduced circulating glucose levels compared with the WT (mixed-effects analysis: F_{6, 150} = 6.616, ####p < 0.0001), resulting in a lower area under the curve of the glucose response (t test: t₂₅ = 4.444, ***p < 0.001).
(G–I) During an ipGTT (2 g/kg glucose) following 14 days of HFD feeding, *Vhl*^{ΔGut} mice have (G) lower circulating glucose levels compared with the WT (mixed-effects analysis: F_{6, 162} = 18.27, ####p < 0.0001), resulting in a lower area under the curve of the glucose response; t test: t₂₇ = 6.487, ****p < 0.0001. Under HFD conditions, *Vhl*^{ΔGut} mice have (H) lower hepatic triglyceride levels (average ± SEM; WT, n = 4; *Vhl*^{ΔGut}, n = 8; t test: t₁₀ = 3.253, **p < 0.01) and (I) lower hepatic total cholesterol levels (t test: t₁₀ = 2.445, **p < 0.05).
(J) *Vhl*^{ΔGut} mice do not have altered circulating iron levels. average ± SEM; WT, n = 71 *Vhl*^{ΔGut}, n = 6.
(K) *Vhl*^{ΔGut} mice have increased circulating hepcidin levels. t test: t₁₂ = 3.943, **p < 0.01.
(L) Following 4 h of fasting, *Vhl*^{ΔGut} mice have increased basal circulating total GLP-1 levels. Average ± SEM; WT, n = 15; *Vhl*^{ΔGut}, n = 15; t test: t₂₇ = 5.689, ****p < 0.001.

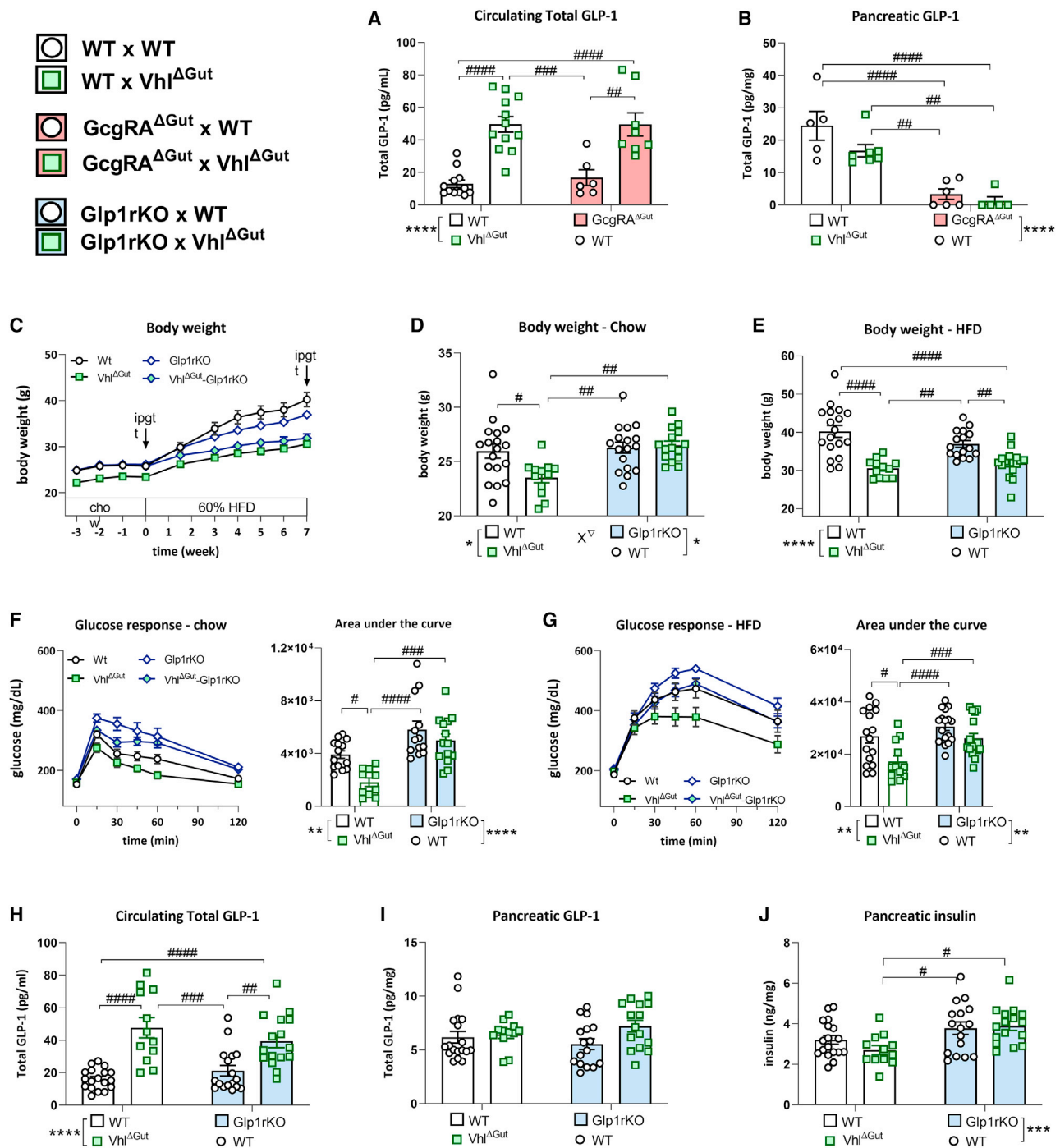


Figure 5. Diet-induced obesity resistance of the $Vhl^{\Delta Gut}$ depends on Glp1R signaling

(A and B) The combination of $Vhl^{\Delta Gut}$ and intestinal Gcg reactivation ($GcgRA^{\Delta Gut}$) show that (A) increased circulating total GLP-1 levels in $Vhl^{\Delta Gut}$ mice (average \pm SEM; WT x WT, n = 12; WT x $Vhl^{\Delta Gut}$, n = 12; $GcgRA^{\Delta Gut}$ x WT, n = 6; $GcgRA^{\Delta Gut}$ x $Vhl^{\Delta Gut}$, n = 8; two-way ANOVA: $F_{1,34} = 48.18$, ****p < 0.0001 effect of $Vhl^{\Delta Gut}$; ####p < 0.0001 post hoc Tukey test) originates from the intestine and not (B) from the pancreas (two-way ANOVA: $F_{1,19} = 53.78$, ****p < 0.0001 effect of $GcgRA^{\Delta Gut}$).

(C) Body weight over the duration of the study reveals that $Vhl^{\Delta Gut}$ mice are lower in body weight while fed a chow diet. During 7 weeks of 60% HFD diet feeding, $Vhl^{\Delta Gut}$ -Glp1rKO mice attenuate weight gain to the level of $Vhl^{\Delta Gut}$ mice, revealing that DIO resistance is not dependent on GLP1R action.

(D) Under standard chow diet conditions, $Vhl^{\Delta Gut}$ mice are lower in body weight compared with WT, Glp1rKO, or $Vhl^{\Delta Gut}$ -Glp1rKO mice. Average \pm SEM; WT x WT, n = 18; WT x $Vhl^{\Delta Gut}$, n = 12; Glp1rKO x WT, n = 16; Glp1rKO x $Vhl^{\Delta Gut}$, n = 15; two-way ANOVA: $F_{1,58} = 5.986$, ∇ p < 0.05 interaction, #p < 0.05, ##p < 0.01 post hoc Tukey test).

(legend continued on next page)

mice have increased circulating total GLP-1 levels (Figure 5H) without increased pancreatic GLP-1 (Figure 5I). Remarkably, under chow conditions, only *Vhl*^{ΔGut} mice are lower in body weight (Figures 5C and 5D) compared with all other groups, revealing that GLP-1 receptor action is essential for the lower-body-weight phenotype of *Vhl*^{ΔGut} mice. However, when switched to a 60% HFD, *Vhl*^{ΔGut} and *Vhl*^{ΔGut}*Glp1r*^{KO} mice show resistance to DIO (Figures 5C and 5E). Because *Glp1r*^{KO} mice are known to be resistant to DIO (Ayala et al., 2010), the decreased weight gain in *Vhl*^{ΔGut}*Glp1r*^{KO} mice cannot be fully attributed to the inhibited action of GLP-1 and may be explained partly by increased pancreatic insulin levels (Figure 5J). Nonetheless, under chow conditions (Figures 5F) and 60% HFD conditions (Figure 5G), *Vhl*^{ΔGut} mice have a lower glucose response compared with *Vhl*^{ΔGut}*Glp1r*^{KO} mice even though body weights were similar between groups following 7 weeks of 60% HFD feeding. These data demonstrate that increased GLP-1R signaling in *Vhl*^{ΔGut} mice is essential for the lean phenotype under chow conditions and improved glucose tolerance under chow as well as HFD conditions.

DISCUSSION

Bariatric surgeries, including VSG, have profound effects on a number of physiological systems. These include obvious ones, such as regulation of food intake and body weight, and less obvious ones, such as the drive to breathe in response to escalating levels of CO₂ (Arble et al., 2019). Here we find that this includes an effect on regulation of iron and HIF in the proximal small intestine. Clinically, bariatric surgeries result in lower circulating iron levels, and this has largely been deemed a result of malabsorption from an altered GI tract that is physically less capable of absorbing iron (Ruz et al., 2009; Steenackers et al., 2018; Gowanlock et al., 2020). In the clinic, individuals undergoing bariatric surgery are given iron supplements to reduce this deleterious effect. In two different models where the ability of VSG to reduce iron levels was abrogated, the benefits of VSG on glucose and body weight were normal. This indicates that the beneficial metabolic effects of VSG are not secondary to lowering iron.

If the effects of VSG are not secondary to reduced circulating iron levels, then the next question is whether intestinal HIF2 α is necessary for the effects of VSG. To test this hypothesis, we created a mouse that had specifically reduced HIF2 α signaling in the intestine. Despite profound reductions in HIF2 α in the duodenum, the ability of VSG to reduce food intake, body weight, and body fat and improve glucose tolerance was normal in intestinal *Hif2 α* ^{ΔGut} mice. These data

make a strong case that HIF2 α is not required for the metabolic effects of VSG. However, there are a number of HIFs expressed in the intestine that share similar signaling pathways; therefore, the potential crosstalk between these pathways may partly compensate for HIF2 α deficiency (Ramakrishnan and Shah, 2017; Xie et al., 2017).

Although HIF2 α is not necessary for the metabolic effects of VSG, the question remains as to whether activation of the HIF2 α pathway will mimic the beneficial effects of VSG on weight, glucose, and gut hormone secretion. To examine this, we took advantage of a mouse where *Vhl* was deleted specifically from the intestine (Shah et al., 2008, 2009). VHL is critical for the effects of HIF2 α (and other HIFs) because it ubiquitinates HIFs and targets them for peroxisomal degradation and, therefore, keeps HIF from entering the nucleus to stimulate target transcription. Through KO of *Vhl*, HIFs are not degraded, and this results in increased target gene transcription. Indeed, intestinal *Vhl*^{ΔGut} mice have profound increases in the expression of several HIF2 α target genes. Moreover, the lean phenotype of these mice is quite profound when they are placed on chow or an HFD. On chow, *Vhl*^{ΔGut} mice are considerably leaner than their littermate controls and have better glucose tolerance. This effect becomes substantially bigger when the mice are placed on an HFD, with ~50% less body fat after 21 days on an HFD (Figure 4E). On an HFD, *Vhl*^{ΔGut} mice have a much lower glucose excursion during a glucose tolerance test compared with their littermate controls (Figure 4G). Even though all intestinal iron transporters are highly upregulated in *Vhl*^{ΔGut} mice, these mice tend to have lower circulating iron levels. This reduction in circulating iron levels is accompanied by significantly higher circulating hepcidin levels, such as what occurs after VSG on a high-iron diet. Finally, we found that *Vhl*^{ΔGut} mice have increased basal GLP-1 levels.

We will admit being surprised by the profound and consistent phenotype of these mice. The selective upregulation of HIF-related signaling in the intestine had a profound effect on several varied parameters that mimic disparate physiologic effects of what occurs after VSG. Among the most curious of these is the robust increase in circulating GLP-1 levels. GLP-1 receptor activation can produce weight loss and glucose improvements in rodents and humans and is the basis for currently approved therapies for obesity and type 2 diabetes (Astrup et al., 2009; Barrera et al., 2011; Burmeister et al., 2012; Heppner and Perez-Tilve, 2015). GLP-1 is just one peptide product of the large pro-hormone *Gcg* (Müller et al., 2019). *Gcg* is expressed in a number of tissues, including the gut, pancreas, and central nervous system. Consequently, we sought to determine whether the increased circulating levels of GLP-1 were derived primarily

(E) Following 7 weeks of 60% HFD feeding, *Vhl*^{ΔGut} are similar in weight to *Vhl*^{ΔGut}-*Glp1r*^{KO} mice. Two-way ANOVA: $F_{1,58} = 40.66$, **** $p < 0.0001$ main effect of *Vhl*^{ΔGut}, # $p < 0.05$, ### $p < 0.001$, #### $p < 0.0001$ post hoc Tukey test.

(F) Under chow conditions, the lower glucose response during an ipGTT (2 g/kg glucose) in *Vhl*^{ΔGut} mice depends on *Glp1r* action. Area under the curve: two-way ANOVA: $F_{1,47} = 29.49$, **** $p < 0.0001$ main effect of *Glp1r*^{KO}, ** $p < 0.01$ main effect of *Vhl*^{ΔGut}, # $p < 0.05$, ### $p < 0.001$, #### $p < 0.0001$ post hoc Tukey test).

(G) Under 60% HFD conditions, the lower glucose response during an ipGTT in *Vhl*^{ΔGut} mice does depend on *Glp1r* action. Area under the curve: two-way ANOVA: $F_{1,58} = 46.75$, **** $p < 0.0001$ main effect of *Vhl*^{ΔGut}; $F_{1,58} = 6.951$, $\nabla p < 0.05$ interaction, ## $p < 0.01$, #### $p < 0.0001$ post hoc Tukey test.

(H and I) *Vhl*^{ΔGut} and *Vhl*^{ΔGut}*Glp1r*^{KO} mice have increased circulating total GLP-1 levels (two-way ANOVA: $F_{1,34} = 48.18$, **** $p < 0.0001$ main effect of *Vhl*^{ΔGut}, # $p < 0.01$, ### $p < 0.001$, #### $p < 0.0001$ post hoc Tukey test) but (I) comparable levels of pancreatic GLP-1.

(J) Pancreatic insulin was higher in the *Glp1r*^{KO} groups compared with *Vhl*^{ΔGut}. Two-way ANOVA: $F_{1,58} = 12.43$, *** $p < 0.001$ main effect of *Glp1r*^{KO}, # $p < 0.05$ post hoc Tukey test).

from the intestine. We crossed $Vhl^{\Delta Gut}$ mice with a mouse where we could selectively reactivate the endogenous *Gcg* allele in the gut (Chambers et al., 2017). In mice where the endogenous allele for *Gcg* was RA only in the intestine, the effect of VHL deficiency to increase basal GLP-1 circulating levels was similar to intestinal VHL deficiency alone.

These data make a compelling case that the increased circulating levels of GLP-1 in $Vhl^{\Delta Gut}$ mice are a product of increased secretion of GLP-1 from the gut. Interpreting other metabolic parameters from these mice is complicated because these mice not only lack GLP-1 but also other *Gcg*-derived peptides. These mice have exceptionally good glucose tolerance, presumably because of their lack of glucagon (Chambers et al., 2017). Consequently, they are a poor model on which to test whether the effect of intestinal VHL deficiency depends on the increased secretion of GLP-1. To test the role of GLP-1 signaling in the phenotype of $Vhl^{\Delta Gut}$ mice, we crossed these mice with GLP-1 receptor KO mice. Again, we observed the effect of intestinal VHL deficiency to increase basal GLP-1 secretion, and this was not altered by KO of the GLP-1 receptor (Figure 5J). Interestingly, loss of GLP-1R signaling completely abrogated the lean phenotype of $Vhl^{\Delta Gut}$ mice on chow but not when switched to an HFD. In the case of glucose levels, loss of GLP-1R signaling clearly abrogated the beneficial effects observed on glucose tolerance in $Vhl^{\Delta Gut}$ mice under both diet conditions.

These data point toward a profound effect of bariatric surgery to increase HIF2 α signaling in the gut. The effect of VSG to lower iron likely depends on the ability of VSG to increase hepcidin secretion from the liver. What remains unclear is how the signal from the surgically altered GI tract affects hepcidin secretion from the liver. However, a wide range of data points to the important effects of VSG to alter liver function, which includes hepatic glucose production (Chambers et al., 2011), bile acid secretion (Myronovych et al., 2014; Ryan et al., 2014), and triglyceride accumulation (Myronovych et al., 2014).

Although the effect of VSG does not depend on HIF2 α activation in the intestine, increasing HIF2 α signaling in the gut by selective disruption of VHL in the intestine results in reduced weight gain and improved glucose tolerance on an HFD. VSG and selective disruption of VHL in the intestine result in increased basal secretion of GLP-1 from the intestine. The improved metabolic phenotype of $Vhl^{\Delta Gut}$ mice does not easily fit with previous observations that expression of HIF2 α in the ileum is positively correlated with increasing BMI and that genetic or pharmacological inhibition of HIF2 α improved metabolism by reducing ceramide levels (Xie et al., 2017). Our work focused on regulation of HIF2 α in the duodenum, whereas the measurements from Xie et al. (2017) were from the ileum. We focused on the duodenum because expression of HIF2 α and many of its key target genes is considerably higher in the duodenum than in the ileum, and this is consistent with its role in iron absorption, which occurs mostly in the duodenum (Figure 1). Moreover, conditional versus constitutive intestine-specific HIF2 α KO used by Xie et al. (2017) could contribute to the discrepancy in metabolic endpoints. Nonetheless, comparable with Xie et al., we also found a reduction of liver triglyceride levels in conditional $Hif2\alpha^{\Delta Gut}$ mice, confirming a role of intestinal *Hif2 α* in liver lipid metabolism.

These data point to a clear effect of multiple bariatric surgeries to increase HIF2 α signaling in the small intestine. The current data indicate that manipulations of HIF2 α signaling, whether they are the result of altered GI anatomy or genetic deletion of VHL, result in similar effects on weight, metabolism, and gut hormone secretion. There are a number of potential ways to manipulate HIF2 α signaling, particularly because the key cells are found facing the lumen in the upper small intestine. Such manipulations could replicate the effects of VSG without the need for permanent alterations of GI anatomy.

Limitations of the study

The experiments described here are technically demanding and occurred over more than a 5-year period and not in the order in which they are now presented. Therefore, not all experimental measurements and timelines are parallel among all experiments. In some cases, the same measurement was made with different assays. Further, the complex breeding involved in the various tissue-specific knockdowns prevented us from having all mice on exactly the same genetic background. All of these issues limit direct comparisons of actual values among the various experiments. Nevertheless, each experiment includes critical control groups to assess the effect of the surgery and genotype and their potential interactions in that experiment. Throughout these experiments, we used mixtures of oral glucose tolerance tests and i.p. glucose tolerance tests. I.p. glucose tolerance tests have the limitation that they do not engage the multiple components of the GI tract that contribute to regulation and potential dysregulation of glucose levels. In all cases, however, we documented the effect of our surgical or genetic manipulation on multiple measures of overall glucose regulation. Finally, it is important to note that VHL's ability to target proteins for degradation are not specific to HIF2 α . VHL is an important component of degradation of various forms of HIF (Shah and Xie, 2014; Yang et al., 2015; Ramakrishnan and Shah, 2016; Xie et al., 2017). Consequently, the substantial phenotype of intestine-specific deletion of VHL cannot be unambiguously attributed entirely to activation of HIF2 α . Although HIF2 α is the logical target, given that its signaling is upregulated exclusively after VSG and RYGB, these experiments cannot exclude the possibility that other targets of VHL may contribute to the observed effects.

STAR★METHODS

Detailed methods are provided in the online version of this paper and include the following:

- KEY RESOURCES TABLE
- RESOURCE AVAILABILITY
 - Lead contact
 - Material availability
 - Data and code availability
- EXPERIMENTAL MODEL AND SUBJECT DETAILS
 - Animal study design
 - Intestinal ODD-luciferase activity following VSG
 - Characterization of $Vhl^{F/F};Vil^{Cre}$ mice
 - Response to VSG in mice fed a high iron containing diet

- Response to VSG in a mouse model of hereditary hemochromatosis
- Response to VSG in intestinal Hif2 α knockout mice
- Origin of increased circulating total GLP-1 in Vhl^{F/F};Vil-CRE mice
- Vhl^{F/F}-Vil^{CRE} mice phenotype dependency on GLP-1 action
- Rat cohort for RNA sequencing study
- **METHOD DETAILS**
 - Genotyping
 - Vertical sleeve gastrectomy surgery (VSG)
 - Glucose tolerance test
 - ELISA
 - Luciferase assay
 - Body composition
 - RT-PCR
 - Transcriptome analysis
- **QUANTIFICATION AND STATISTICAL ANALYSIS**
 - Statistics

SUPPLEMENTAL INFORMATION

Supplemental information can be found online at <https://doi.org/10.1016/j.celrep.2021.110270>.

ACKNOWLEDGMENTS

This work was supported by University of Michigan DK020572 (MDRC), DK089503 (MNORC), NIH 5T32DK108740 (to N.B.-K.), 5T32DK071212-12 (to N.B.-K.), UL1TR002240 (to N.B.-K.), a China Scholarship Council grant (CSC#201606100218 to Y.S.), DK110537 (to S.K.R.), R01CA148828, R01DK095201, R01CA245546, GI Center P30DK034933 (to Y.M.S.), German Research Foundation grant SFB 1321/1 and German Center for Diabetes Research (to K.S.), and the Helmholtz Alliance “Aging and Metabolic Programming, AMPPro” (to M.I. from support of Johannes Beckers). We would also like to thank Drs. Alfor Lewis, Andriy Myronovich, and Mouhamadou Toure for the extensive surgical work on this project and Kelli Rule and Jack Magrisso for work on the mouse models. We would also like to thank Johannes Beckers for critical work on the arrays to identify gene similarities between VSG and RYGB.

AUTHOR CONTRIBUTIONS

Conceptualization, S.S.E., S.K.R., Y.M.S., and R.J.S.; formal analysis, M.I., K.S., S.S.E., and Y.S.; investigation, S.S.E., Y.S., S.K.R., J.H.S., and N.B.-K.; resources, D.A.S.; data curation, S.S.E., Y.S., S.K.R., M.I., and K.S.; writing – original draft, S.S.E., Y.S., S.K.R., Y.M.S., and R.J.S.; writing – review & editing, S.S.E., Y.S., S.K.R., J.H.S., N.B.-K., M.I., K.S., D.A.S., Y.M.S., and R.J.S.; visualization, S.S.E., Y.S., M.I., and K.S.

DECLARATION OF INTERESTS

R.J.S. has received research support from Novo Nordisk, Astra Zeneca, Pfizer, Energesis, Kintai, and Ionis. R.J.S. has served as a paid consultant for Novo Nordisk, Scobia, Kintai, Eli Lilly, and Ionis. R.J.S. has equity positions in Calibrate and Rewind.

Received: April 22, 2021
Revised: September 11, 2021
Accepted: December 23, 2021
Published: January 18, 2022

REFERENCES

- Aarts, E.O., Janssen, I.M.C., and Berends, F.J. (2011). The gastric sleeve: losing weight as fast as micronutrients? *Obes. Surg.* 21, 207–211. <https://doi.org/10.1007/s11695-010-0316-7>.
- Abu-Gazala, S., Horwitz, E., Ben-Haroush Schyr, R., Bardugo, A., Israeli, H., Hija, A., Schug, J., Shin, S., Dor, Y., and Kaestner, K.H. (2018). Sleeve gastrectomy improves glycemia independent of weight loss by restoring hepatic insulin sensitivity. *Diabetes* 67, 1079–1085. <https://doi.org/10.2337/db17-1028>.
- Anderson, E.R., Taylor, M., Xue, X., Ramakrishnan, S.K., Martin, A., Xie, L., Bredell, B.X., Gardenghi, S., Rivella, S., and Shah, Y.M. (2013). Intestinal HIF2 α promotes tissue-iron accumulation in disorders of iron overload with anemia. *Proc Natl Acad Sci U S A* 110, 4922–30. <https://doi.org/10.1073/pnas.1314197110>.
- Arble, D.M., Evers, S.S., Bozadjieva, N., Frikke-Schmidt, H., Myronovych, A., Lewis, A., Toure, M.H., and Seeley, R.J. (2018). Metabolic comparison of one-anastomosis gastric bypass, single-anastomosis duodenal-switch, Roux-en-Y gastric bypass, and vertical sleeve gastrectomy in rat. *Surg. Obes. Relat. Dis.* 14, 1857–1867. <https://doi.org/10.1016/j.soard.2018.08.019>.
- Arble, D.M., Schwartz, A.R., Polotsky, V.Y., Sandoval, D.A., and Seeley, R.J. (2019). Vertical sleeve gastrectomy improves ventilatory drive through a leptin-dependent mechanism. *JCI Insight* 4. <https://doi.org/10.1172/jci.insight.124469>.
- Astrup, A., Rössner, S., Van Gaal, L., Rissanen, A., Niskanen, L., Al Hakim, M., Madsen, J., Rasmussen, M.F., and Lean, M.E. (2009). Effects of liraglutide in the treatment of obesity: a randomised, double-blind, placebo-controlled study. *Lancet* 374, 1606–1616. [https://doi.org/10.1016/S0140-6736\(09\)61375-1](https://doi.org/10.1016/S0140-6736(09)61375-1).
- Ayala, J.E., Bracy, D.P., James, F.D., Burmeister, M.A., Wasserman, D.H., and Drucker, D.J. (2010). Glucagon-like peptide-1 receptor knockout mice are protected from high-fat diet-induced insulin resistance. *Endocrinology* 151, 4678–4687. <https://doi.org/10.1210/en.2010-0289>.
- Barrera, J.G., Sandoval, D.A., D'Alessio, D.A., and Seeley, R.J. (2011). GLP-1 and energy balance: an integrated model of short-term and long-term control. *Nat Rev Endocrinol* 7, 507–516. <https://doi.org/10.1038/nrendo.2011.77>.
- Ben-Zvi, D., Meoli, L., Abidi, W.M., Nestoridi, E., Panciotti, C., Castillo, E., Pizarro, P., Shirley, E., Gourash, W.F., Thompson, C.C., et al. (2018). Time-dependent molecular responses differ between gastric bypass and dieting but are conserved across species. *Cell Metab.* 28, 310–323.e6. <https://doi.org/10.1016/j.cmet.2018.06.004>.
- Burmeister, M.A., Ferre, T., Ayala, J.E., King, E.M., Holt, R.M., and Ayala, J.E. (2012). Acute activation of central GLP-1 receptors enhances hepatic insulin action and insulin secretion in high-fat-fed, insulin resistant mice. *Am. J. Physiol. Endocrinol. Metab.* 302, E334–E343. <https://doi.org/10.1152/ajpendo.00409.2011>.
- Chambers, A.P., Jessen, L., Ryan, K.K., Sisle, S., Wilson-Pérez, H.E., Stefater, M.A., Gaitonde, S., Sorrell, J.E., Toure, M., Berger, J., et al. (2011). Weight-independent changes in blood glucose homeostasis after gastric bypass or vertical sleeve gastrectomy in rats. *Gastroenterology* 141, 950–958. <https://doi.org/10.1053/j.gastro.2011.05.050>.
- Chambers, A.P., Sorrell, J.E., Haller, A., Roelofs, K., Hutch, C.R., Kim, K.S., Gutierrez-Aguilar, R., Li, B., Drucker, D.J., D'Alessio, D.A., et al. (2017). The role of pancreatic preproglucagon in glucose homeostasis in mice. *Cell Metab.* 25, 927–934.e3. <https://doi.org/10.1016/j.cmet.2017.02.008>.
- Cummings, D.E., Arterburn, D.E., Westbrook, E.O., Kuzma, J.N., Stewart, S.D., Chan, C.P., Bock, S.N., Landers, J.T., Kratz, M., Foster-Schubert, K.E., et al. (2016). Gastric bypass surgery vs intensive lifestyle and medical intervention for type 2 diabetes: the CROSSROADS randomised controlled trial. *Diabetologia* 59, 945–953. <https://doi.org/10.1007/s00125-016-3903-x>.

- Das, N.K., Shwartz, A.J., Barthel, G., Inohara, N., Liu, Q., Sankar, A., Hill, D.R., Ma, X., Lamberg, O., Schnizlein, M.K., et al. (2019). Microbial metabolite signaling is required for systemic iron homeostasis. *Cell Metab.* <https://doi.org/10.1016/j.cmet.2019.10.005>.
- Evers, S.S., Kim, K.-S., Bozadjieva, N., Lewis, A.G., Farris, D., Sorensen, M.J., Kim, Y., Whitesall, S.E., Kennedy, R.T., Michele, D.E., et al. (2019). Continuous glucose monitoring reveals glycemic variability and hypoglycemia after vertical sleeve gastrectomy in rats. *Mol. Metabol.* *32*, 148–159. <https://doi.org/10.1016/j.molmet.2019.12.011>.
- Ganz, T., and Nemeth, E. (2012). Hcpidin and iron homeostasis. *Biochim. Biophys. Acta (BBA) Mol. Cell Res.* *1823*, 1434–1443. <https://doi.org/10.1016/j.bbamcr.2012.01.014>.
- Gowanlock, Z., Lezhanska, A., Conroy, M., Crowther, M., Tiboni, M., Mbuagbaw, L., and Siegal, D.M. (2020). Iron deficiency following bariatric surgery: a retrospective cohort study. *Blood Adv.* *4*, 3639–3647. <https://doi.org/10.1182/bloodadvances.2020001880>.
- Heppner, K.M., and Perez-Tilve, D. (2015). GLP-1 based therapeutics: simultaneously combating T2DM and obesity. *Front. Neurosci.* *9*. <https://doi.org/10.3389/fnins.2015.00092>.
- Kotkiewicz, A., Donaldson, K., Dye, C., Rogers, A.M., Mauger, D., Kong, L., and Eyster, M.E. (2015). Anemia and the need for intravenous iron infusion after roux-en-Y gastric bypass. *Clin. Med. Insights Blood Disord.* *8*. <https://doi.org/10.4137/CMBD.S21825>.
- Lando, D., Peet, D.J., Whelan, D.A., Gorman, J.J., and Whitelaw, M.L. (2002). Asparagine hydroxylation of the HIF transactivation domain a hypoxic switch. *Science* *295*, 858–861. <https://doi.org/10.1126/science.1068592>.
- Lane, D.J., Bae, D.H., Merlot, A.M., Sahni, S., and Richardson, D.R. (2015). Duodenal cytochrome b (DCYTB) in iron metabolism: an update on function and regulation. *Nutrients* *7*, 2274–2296. <https://doi.org/10.3390/NU7042274>.
- Lee, P., Chandel, N.S., and Simon, M.C. (2020). Cellular adaptation to hypoxia through hypoxia inducible factors and beyond. *Nat. Rev. Mol. Cell Biol.* *21*, 268–283. <https://doi.org/10.1038/s41580-020-0227-y>.
- Mastrogiannaki, M., Matak, P., Keith, B., Simon, M.C., Vaulont, S., and Peyssonnaud, C. (2009). HIF-2 α , but not HIF-1 α , promotes iron absorption in mice. *J. Clin. Invest.* *119*, 1159–1166. <https://doi.org/10.1172/JCI38499>.
- Mechanick, J.I., Apovian, C., Brethauer, S., Garvey, W.T., Joffe, A.M., Kim, J., Kushner, R.F., Lindquist, R., Pessah-Pollack, R., Seger, J., et al. (2020). Clinical practice guidelines for the perioperative nutrition, metabolic, and nonsurgical support of patients undergoing bariatric procedures - 2019 update: co-sponsored by American Association of Clinical Endocrinologists/American College of Endocrinology, The Obesity Society, American Society for Metabolic & Bariatric Surgery, Obesity Medicine Association, and American Society of Anesthesiologists. *Surg. Obes. Relat. Dis.* *16*, 175–247. <https://doi.org/10.1016/j.soard.2019.10.025>.
- Mingrone, G., Panunzi, S., De Gaetano, A., Guidone, C., Iaconelli, A., Capristo, E., Chamseddine, G., Bornstein, S.R., and Rubino, F. (2021). Metabolic surgery versus conventional medical therapy in patients with type 2 diabetes: 10-year follow-up of an open-label, single-centre, randomised controlled trial. *Lancet.* *397*, 293–304. [https://doi.org/10.1016/S0140-6736\(20\)32649-0](https://doi.org/10.1016/S0140-6736(20)32649-0).
- Mischler, R.A., Armah, S.M., Craig, B.A., Rosen, A.D., Banerjee, A., Selzer, D.J., Choi, J.N., and Gletsu-Miller, N. (2018). Comparison of oral iron supplement formulations for normalization of iron status following roux-EN-y gastric bypass surgery: a randomized trial. *Obes. Surg.* *28*, 369–377. <https://doi.org/10.1007/s11695-017-2858-4>.
- Müller, T.D., Finan, B., Bloom, S.R., D'Alessio, D., Drucker, D.J., Flatt, R.R., Fritsche, A., Gribble, F., Grill, H.J., Habener, J.F., et al. (2019). Glucagon-like peptide 1 (GLP-1). *Mol. Metab.*, 72–130. <https://doi.org/10.1016/j.molmet.2019.09.010>.
- Myronovych, A., Kirby, M., Ryan, K.K., Zhang, W., Jha, P., Setchell, K.D., Dexheimer, P.J., Aronow, B., Seeley, R.J., and Kohli, R. (2014). Vertical sleeve gastrectomy reduces hepatic steatosis while increasing serum bile acids in a weight-loss-independent manner. *Obesity* *22*, 390–400. <https://doi.org/10.1002/oby.20548>.
- R Core Team (2017). R A Language and Environment for Statistical Computing. - References - Scientific Research Publishing (No Date), . [https://www.scirp.org/\(S\(351jmbntvnsjt1aadkposzje\)\)/reference/ReferencesPapers.aspx?ReferenceID=2144573](https://www.scirp.org/(S(351jmbntvnsjt1aadkposzje))/reference/ReferencesPapers.aspx?ReferenceID=2144573)
- Rainer, J., Sanchez-Cabo, F., Stocker, G., Sturn, A., and Trajanoski, Z. (2006). CARMAweb: comprehensive R- and bioconductor-based web service for microarray data analysis. *Nucleic Acids Res.* *34*, W498–W503, (WEB. SERV. ISS.). <https://doi.org/10.1093/nar/gkl038>.
- Ramakrishnan, S.K., and Shah, Y.M. (2016). Role of intestinal HIF-2 α in health and Disease. *Annu. Rev. Physiol.* *78*, 301–325. <https://doi.org/10.1146/annurev-physiol-021115-105202>.
- Ramakrishnan, S.K., and Shah, Y.M. (2017). A central role for hypoxia-inducible factor (HIF)-2 α in hepatic glucose homeostasis. *Nutr. Health. Aging*, 207–216. <https://doi.org/10.3233/NHA-170022>.
- Richards, P., Parker, H.E., Adriaenssens, A.E., Hodgson, J.M., Cork, S.C., Trapp, S., Gribble, F.M., and Reimann, F. (2014). Identification and characterization of GLP-1 receptor-expressing cells using a new transgenic mouse model. *Diabetes* *63*, 1224–1233. <https://doi.org/10.2337/db13-1440>.
- le Roux, C.W., and Bueter, M. (2014). The physiology of altered eating behaviour after Roux-en-Y gastric bypass. *Exp. Physiol.* *99*, 1128–1132. <https://doi.org/10.1113/expphysiol.2014.078378>.
- Ruz, M., Carrasco, F., Rojas, P., Codoceo, J., Inostroza, J., Rebolledo, A., Basfi-fer, K., Csendes, A., Papapietro, K., Pizarro, F., et al. (2009). Iron absorption and iron status are reduced after Roux-en-Y gastric bypass. *Am. J. Clin. Nutr.* *90*, 527–532. <https://doi.org/10.3945/ajcn.2009.27699>.
- Ryan, K.K., Tremaroli, V., Clemmensen, C., Kovatcheva-Datchary, P., Myronovych, A., Karns, R., Wilson-Pérez, H.E., Sandoval, D.A., Kohli, R., et al. (2014). FXR is a molecular target for the effects of vertical sleeve gastrectomy. *Nature* *509*, 183–188. <https://doi.org/10.1038/nature13135>.
- Schauer, P.R., Bhatt, D.L., Kirwan, J.P., Wolski, K., Aminian, A., Brethauer, S.A., Navaneethan, S.D., Singh, R.P., Pothier, C.E., Nissen, S.E., et al. (2017). Bariatric surgery versus intensive medical therapy for diabetes — 5-year outcomes. *N. Engl. J. Med.* *376*, 641–651. <https://doi.org/10.1056/nejmoa1600869>.
- Shah, Y.M., Ito, S., Morimura, K., Chen, C., Yim, S.H., Haase, V.H., and Gonzalez, F.J. (2008). Hypoxia-inducible factor Augments experimental colitis through an MIF-dependent Inflammatory signaling Cascade. *Gastroenterology* *134*, 2036–2048. <https://doi.org/10.1053/j.gastro.2008.03.009>.
- Shah, Y.M., Matsubara, T., Ito, S., Yim, S.H., and Gonzalez, F.J. (2009). Intestinal hypoxia-inducible transcription factors are essential for iron absorption following iron deficiency. *Cell Metab.* *9*, 152–164. <https://doi.org/10.1016/j.cmet.2008.12.012>.
- Shah, Y.M., and Xie, L. (2014). Hypoxia-inducible factors link iron homeostasis and erythropoiesis. *Gastroenterology* *146*, 630–642. <https://doi.org/10.1053/j.gastro.2013.12.031>.
- Steenackers, N., Van der Schueren, B., Mertens, A., Lannoo, M., Grauwet, T., Augustijns, P., and Matthys, C. (2018). Iron deficiency after bariatric surgery: what is the real problem? *Proc. Nutr. Soc.* *77*, 1445–1455. <https://doi.org/10.1017/S0029665118000149>.
- Stéfater, M.A., Pérez-Tilve, D., Chambers, A.P., Wilson-Pérez, H.E., Sandoval, D.A., Berger, J., Toure, M., Tschöp, M., Woods, S.C., and Seeley, R.J. (2010). Sleeve Gastrectomy Induces Loss of Weight and Fat Mass in Obese Rats, but Does Not Affect Leptin Sensitivity. *Gastroenterology* *138*, 2426–2436. <https://doi.org/10.1053/j.gastro.2010.02.059>.
- Taylor, M., Qu, A., Anderson, E.R., Matsubara, T., Martin, A., Gonzalez, F.J., and Shah, Y.M. (2011). Hypoxia-inducible factor-2 α mediates the adaptive increase of intestinal ferroportin during iron deficiency in mice. *Gastroenterology* *140*, 2044–2055. <https://doi.org/10.1053/j.gastro.2011.03.007>.

Welbourn, R., Hollyman, M., Kinsman, R., Dixon, J., Liem, R., Ottosson, J., Ramos, A., Våge, V., Al-Sabah, S., Brown, W., et al. (2019). Bariatric surgery Worldwide: baseline demographic description and one-year outcomes from the Fourth IFSO Global Registry report 2018. *Obes. Surg.* *29*, 782–795. <https://doi.org/10.1007/s11695-018-3593-1>.

Xie, C., Yagai, T., Luo, Y., Liang, X., Chen, T., Wang, Q., Sun, D., Zhao, J., Ramakrishnan, S.K., Sun, L., et al. (2017). Activation of intestinal hypoxia-inducible

factor 2 α during obesity contributes to hepatic steatosis. *Nat. Med.* *23*, 1298–1308. <https://doi.org/10.1038/nm.4412>.

Yang, S.L., Wu, C., Xiong, Z.F., and Fang, X. (2015). Progress on hypoxia-inducible factor-3: its structure, gene regulation and biological function (Review). *Mol. Med. Rep.* *12*, 2411–2416. <https://doi.org/10.3892/MMR.2015.3689/HTML>.

STAR★METHODS

KEY RESOURCES TABLE

REAGENT or RESOURCE	SOURCE	IDENTIFIER
Chemicals, peptides, and recombinant proteins		
T-PER Tissue Protein Extraction Reagent	Thermo Fisher Scientific	Cat# 78510
protease inhibitor (1 pill/100ml T-PER)	Sigma-Aldrich	Cat# S8820
DPP-4 inhibitor (20 μ l/ml T-PER)	Millipore-Sigma	Cat# SKUDPP4
BCA protein analysis	Pierce-Fisher	Cat#23225
FailSafe PCR PreMix	Lucigen Corp, Middleton,WI	Cat# FS99250
SYBR Safe	Invitrogen	Cat# S33102
TRIzol reagent	Thermo Fisher Scientific	Cat# 15596026
PureLink RNA mini kit	Thermo Fisher Scientific	Cat# K157001
RNeasy Mini kit	Qiagen	Cat#74106
iScript cDNA synthesis kit	BioRad	Cat# 1708891
SsoAdvanced Universal Probes Supermix	BioRad	Cat# 1725281
Critical commercial assays		
Dual Dual-Luciferase Assay System	Promega	Cat# E1910
Ultra-Sensitive Mouse Insulin ELISA	Crystal Chem	Cat# 90080
QuantiChrom Iron Assay	BioAssay Systems	Cat# DIFE-250
Hepcidin-Murine Compete TM ELISA	Intrinsic Life Sciences	Cat# HMC-001
V-PLEX GLP-1 Total Kit	Meso Scale Discovery	Cat# K1503PD
TaqMan gene expression Assay - Hif2a (Epas1)	ThermoFisher Scientific	Mm01236112_m1
TaqMan gene expression Assay - Hif1a	ThermoFisher Scientific	Mm00468869_m1
TaqMan gene expression Assay - Vhl	ThermoFisher Scientific	Mm00494137_m1
TaqMan gene expression Assay - Dmt1 (Slc11a2)	ThermoFisher Scientific	Mm00435363_m1
TaqMan gene expression Assay - Dcytb (Cybrd1)	ThermoFisher Scientific	Mm01335930_m1
TaqMan gene expression Assay - Phd2 (Egn1)	ThermoFisher Scientific	Mm00459770_m1
TaqMan gene expression Assay - Neu3	ThermoFisher Scientific	Mm00479379_m1
TaqMan gene expression Assay - Pdk1	ThermoFisher Scientific	Mm01276567_m1
TaqMan gene expression Assay - Pdk1	ThermoFisher Scientific	Mm00435617_m1
TaqMan gene expression Assay - Glut1 (Slc2a1)	ThermoFisher Scientific	Mm05908127_s1
TaqMan gene expression Assay - Rpl32	ThermoFisher Scientific	Mm07306626_gH
TaqMan gene expression Assay - Actb	ThermoFisher Scientific	Mm02619580_g1
Deposited data		
Array data submitted to GEO database	This paper	GSE169403
Experimental models: Organisms/strains		
Vhl ^{F/F;Vilcre}	Prof.dr. Y. Shah, Dept. Mol & Int Phys, University of Michigan	N/A
Hif2 α ^{F/F} ;Vil ^{Wt/Wt} , Hif2 α ^{F/F} -Vil ^{CreERT}	Prof.dr. Y. Shah, Dept. Mol & Int Phys, University of Michigan	N/A
Hamp ^{F/F} ;Alb ^{Wt/Wt} Hamp ^{F/F} -Alb ^{Cre}	Prof.dr. Y. Shah, Dept. Mol & Int Phys, University of Michigan	N/A

(Continued on next page)

Continued		
REAGENT or RESOURCE	SOURCE	IDENTIFIER
Gcg ^{stopfloX}	Prof.dr. R.J. Seeley, Dept. Surgery, University of Michigan	N/A
Glp1r ^{stopfloX}	Prof.dr. R.J. Seeley, Dept. Surgery, University of Michigan	N/A
FVB.129S6Gt(ROSA)26Sor ^{tm2(HIF1A/luc)Kael1} J – ODD-Luc	Jackson laboratory	Stock no.006206
C57BL/6J	Jackson Laboratory	Stock no.000664
Long-Evans rats	Harlan Laboratories	HsdBlu: LE
Oligonucleotides		
Oligonucleotides are listed in Table S7	N/A	N/A
Software and algorithms		
Graphpad Prism	Graphpad Software	Version 8.1.2
R A Language and Environment for Statistical Computing	R	R Core Team (2017)
Expression console v.1.3.0.187	Thermo Fisher Scientific	N/A
CARMAweb	Medical University Innsbruck	Rainer et al. (2006)
QIAGEN Ingenuity Pathway Analysis, IPA	QIAGEN	www.qiagen.com/ingenuity
Other		
Regular chow diet	Envigo Teklad	Cat# 7012
60% HFD	Research Diets, Inc	Cat# D12492
Custom high fat (45% FDC) AIN-93G with 35ppm Fe	Dyets Inc, Pa	Cat# 115244
Custom high fat (45% FDC) AIN-93G with 350ppm Fe	Dyets Inc, Pa	Cat# 115245
Osmolite OneCal liquid diet	Abbott, Columbus, OH	Cat# 64633
Ensure Plus	Abbott	Cat # 57263
Accu-Chek Aviva Meter	Accu-Chek, Roche Diabetes Care	https://www.accu-chek.com
Endopath ETS-FLEX 35mm Stapler	Ethicon endo-surgery	VASECR35
Nuclear Magnetic Resonance	EchoMRI LLC, USA	EchoMRI-900
Ovation PicoSL WTA System V2	Nugen	Part no. 3312
GeneChip Rat Gene 2.1 ST Array Plate	Thermofisher Scientific	Cat# 902143

RESOURCE AVAILABILITY

Lead contact

Further information and requests for resources and reagents should be directed to and will be fulfilled by the Lead Contact, Randy J. Seeley (seeleyrj@med.umich.edu).

Material availability

Mouse lines generated in this study have not been deposited. Sources for breeding pairs are available in the [key resources table](#). Requests for available resources (mouse lines, tissue samples, etc.) and reagents should be directed to and will be fulfilled by the lead contact.

Data and code availability

- Standardized RNA sequencing data have been deposited at GEO data base (GSE169403) and are publicly available as of the date of publication. Accession numbers are listed in the [key resources table](#).
- This paper does not report original code.
- Any additional information required to reanalyze the data reported in this paper is available from the lead contact upon request.

EXPERIMENTAL MODEL AND SUBJECT DETAILS

Animal study design

All animal studies were approved by and conducted according to the guidelines of the Institutional Animal Care and Use Committee at the University of Michigan.

Intestinal ODD-luciferase activity following VSG

Male ODD-luciferase reporter mice (FVB.129S6Gt(ROSA)26Sor^{tm2(HIF1A/luc)Kael/J}) at age 4–5 weeks were purchased from Jackson Laboratory. All mice had continuous access to 60% HFD (Research Diets) and water. Mice received either Sham (n=8) or VSG (n=13) following 8 weeks of diet induction and were terminated at 28 days post-surgery. Tissue luciferase activity was measured by homogenizing the tissues with the Dual Dual-Luciferase Assay System (Promega) according to the manufacturer's instructions and measured with SpectraMax M5 (Molecular Devices, San Jose, CA).

Characterization of Vhl^{F/F};Vil^{Cre} mice

Breeder mice were kindly provided by Dr. Y.M Shah from the department of Molecular & Integrative Physiology at the University of Michigan. Prior to study, male Vhl^{F/F};Vil^{Cre} (intestinal Vhl knockout) and wildtype Vhl^{F/F} male littermate mice, had ad lib access to water and regular chow diet (Envigo Teklad). At study day 0, age 10–12 weeks, the diet was switched to a 60% HFD (Research Diets). At study day -1 and day 14 an ip-gtt (2 g/kg glucose) was performed. At day 21 following an overnight fast, animals were euthanized using CO₂ and cardiac puncture. Whole blood was divided of EDTA coated tubes for Heparin and Total GLP-1 analysis and a heparin coated tube for plasma iron analysis. Blood samples were centrifuged at 3000g for 10min at 4°C. Plasma was stored at -80°C until further analysis. Duodenum and ileum were dissected and processed for mRNA expression determination (detailed description below).

Response to VSG in mice fed a high iron containing diet

Male C57B6/J mice (Jackson Laboratory), age 5 weeks at arrival had ad lib access for 6 weeks to 45% high-fat regular iron diet (35ppm Fe, Dyets Inc, #115244) and water before being randomized to 4 groups based on body weight. The groups consisted of two groups receiving Sham surgery of which one group was kept on the 45% high-fat regular iron diet and the other was switched to a 45% high-fat high iron diet (350ppm Fe, Dyets Inc, #115245), the other two groups received VSG surgery (details are described below) of which one group was kept on the 45% high-fat regular iron diet and the other was switched to 45% high-fat regular iron diet. Designated high iron diet groups were switched to the diet 2 weeks prior to surgery. At 56 days post-surgery an ip-gtt (2g/kg glucose) was performed. Animals were terminated at day 70 post surgery using CO₂ and cardiac puncture. Animals were not fasted before termination. At termination, blood was collected to determine hematocrit, total iron levels, and hepcidin levels. Duodenum and ileum were dissected and processed for mRNA expression determination (detailed description below).

Response to VSG in a mouse model of hereditary hemochromatosis

Breeder (Hamp^{F/F};Alb^{Wt/Wt} and Hamp^{F/F}-Alb^{Cre}) mice were kindly provided by Dr. Y.M Shah from the department of Molecular & Integrative Physiology at the University of Michigan. Male offspring were single housed (age 4–5 weeks) and had ad lib access to 60% high fat diet (Research Diets) and water. Following 8 weeks of diet induction mice were randomized to 4 groups of which 2 received Sham surgery, namely Wt-Sham (Hamp^{F/F};Alb^{Wt/Wt}) and Heparin^{ΔLiver}-Sham (Hamp^{F/F};Alb^{Cre}) and 2 groups received VSG surgery, namely Wt-VSG (Hamp^{F/F};Alb^{Wt/Wt}) and Heparin^{ΔLiver}-VSG (Hamp^{F/F};Alb^{Cre}). An ip-gtt (2 g/kg glucose) was performed at 5 weeks post-surgery. Following an overnight fast, animals were terminated 8 weeks post-surgery using CO₂ and cardiac puncture. A whole blood sample (150μl) was collected in a heparin coated tube and send to Unit for Laboratory Animal Medicine (ULAM) at the University of Michigan for the analysis of circulating iron levels, total iron binding capacity (TIBC) and transferrin saturation (%).

Response to VSG in intestinal Hif2α knockout mice

Breeder (Hif2α^{F/F};Vil^{Wt/Wt} and Hif2α^{F/F}-Vil^{CreERT}) mice were kindly provided by Dr. Y.M Shah from the department of Molecular & Integrative Physiology at the University of Michigan. Male offspring were single housed (age 4–5 weeks) and had ad lib access to 60% high fat diet (Research Diets) and water throughout the study. At 6 weeks of diet induction, two weeks prior to surgery, all mice received three doses of tamoxifen (s.c. 10mg/kg) with one day in between each dose to knock down Hif2α expression in villin expressing cells. The study consisted of 4 groups of which 2 received Sham surgery, namely Wt-Sham (Hif2α^{F/F};Vil^{Wt/Wt}) and IntHif2αKO-Sham (Hif2α^{F/F};Vil^{CreERT}) and 2 groups received VSG surgery, namely Wt-VSG (Hif2α^{F/F};Vil^{Wt/Wt}) and IntHif2αKO-VSG (Hif2α^{F/F};Vil^{CreERT}). At 28 days post-surgery, animals received an oral administration of EnsurePlus+2g/kg glucose to measure the Total GLP-1 response at 15min post administration. At 56 days post-surgery an ip-gtt (2 g/kg glucose) was performed. Following an overnight fast, animals were terminated at day 70 post-surgery using CO₂ and cardiac puncture. Duodenum and ileum were dissected and processed for mRNA expression determination (detailed description below).

Origin of increased circulating total GLP-1 in Vhl^{F/F};Vil^{Cre} mice

To study the origin of increased total GLP-1 levels in Vhl^{F/F};Vil^{Cre} mice, we crossbred Vhl^{F/F};Vil^{Cre} with Gcg^{stopflox} mice. Gcg^{stopflox} mice are functionally total body Gcg knockout mice and crossbreeding with Vil^{Cre} mice would result in mice in which Gcg expression

is reactivated (GcgRA) only in the Villin expressing intestinal cells. This resulted in 4 genetically different groups, namely Wt (Vhl^{F/F}; Gcg^{Wt/Wt-Vil^{Wt/Wt}}), Vhl-KO (Vhl^{F/F}; Gcg^{Wt/Wt-Vil^{Cre}}), GcgRA Vhl^{Wt/Wt}; Gcg^{stopflox-Vil^{Cre}}, and VhlKO-GcgRA Vhl^{F/F}; Gcg^{stopflox-Vil^{Cre}}. At 6 weeks of age male offspring were terminated following an overnight fast using CO₂ and cardiac puncture. Blood samples were collected for the determination of Total GLP-1. The pancreas was dissected and flash frozen in liquid nitrogen. Frozen pancreas was first grinded using a mortar and pestle and was lysed in 1mL T-PER Tissue Protein Extraction Reagent (Thermo Fisher Scientific) containing a protease inhibitor cocktail (Sigma-Aldrich; 1 pill/100ml T-PER) and DPP-4 inhibitor (Millipore-Sigma, 20μl/ml T-PER). Samples were centrifuged at 10000g for 5min at 4°C. The supernatant was collected to determine total protein concentration using BCA protein analysis (#23225, Pierce-Fisher) and Total GLP-1 analysis (specified description below).

Vhl^{F/F}-Vil^{Cre} mice phenotype dependency on GLP-1 action

To study the functionality of increased total GLP-1 levels in Vhl^{F/F};Vil^{Cre} mice, we crossbred Vhl^{F/F}-Vil^{Cre} with Glp1r^{stopflox} mice. Glp1r^{stopflox} mice are functionally total body Glp1 receptor knockout mice and crossbreeding with Vil^{Cre} mice would result in mice in which Glp1r expression is reactivated only in the Villin expressing intestinal cells. Because Glp1r is to the best of our knowledge not or barely expressed in intestinal cells (Richards et al., 2014), crossbreeding with Vhl^{Cre} mice would result in a functional total body GLP1r knockout mouse (Glp1rKO). This resulted in 4 genetically different groups, namely Wt (Vhl^{F/F}-Glp1r^{Wt/Wt-Vil^{Wt/Wt}}), Vhl-KO (Vhl^{F/F}-Glp1r^{Wt/Wt-Vil^{Cre}}), Glp1rKO (Vhl^{Wt/Wt}-Glp1r^{stopflox-Vil^{Cre}}), and VhlKO-Glp1rKO (Vhl^{F/F}-Glp1r^{stopflox-Vil^{Cre}}). At age 4-5 weeks, male mice were single housed and had ad lib access to chow and water. An ip-gtt (2 g/kg glucose) was performed 1 week prior and 4 weeks following the switch to a 60% HFD (Research Diets). Following an overnight fast, mice were terminated following 7 weeks of 60% HFD feeding using CO₂ and cardiac puncture. Blood samples were collected for the determination of Total GLP-1 levels.

Rat cohort for RNA sequencing study

Male Long-Evans rats (250 – 300 g, 8 –10 weeks of age; Harlan Laboratories, Indianapolis, IN) were single housed at the Metabolic Diseases Institute of the University of Cincinnati under standard controlled conditions (12:12-h light-dark cycle, 50–60% humidity, 25°C). Animals had free access to water and a high-fat diet (HFD) (40% fat; 4.54 kcal/g, D03082706; Research Diets, New Brunswick, New Jersey) for eight weeks. Three days pre-operatively, rats were matched for body weight and fat mass and randomized to RYGB, VSG, RYGB-sham, and VSG-sham surgical groups (n=6) and the high-fat diet was replaced with Osmolite OneCal liquid diet (Abbott, Columbus, OH). VSG and RYGB surgery were performed in anesthetized rats as described previously (Chambers et al., 2011). All surgical groups received postoperative care consisting of subcutaneous injections of Metacam (0.25 mg/100 g body weight once daily for 4 days), Buprenex (0.3 mL twice a day for 5 days), and warm saline (10 mL and 5 mL twice daily for days 0–3 and 4–5, respectively). During the 5 days of postoperative care, rats had free access to Osmolite OneCal Liquid Diet (Abbott, Columbus, OH) until they were switched back to solid HFD diet. All rats were sacrificed 30 days after surgery.

METHOD DETAILS

Genotyping

Mice were genotyped based on DNA extraction of the tail tip using HotSHOT genomic DNA preparations. In short, tail tips were submerged in 75μl alkaline lysis buffer (125μl 10N NaOH+20μl 0.5M EDTA+50mlH₂O) and heated to 95°C for 30min and cooled to 4°C until 75μl neutralization buffer (325mg Tris-HCl+50ml H₂O) was added to each sample. For PCR, 1-5μl DNA template was used and mixed with FailSafe PCR PreMix (Lucigen Corp, Middleton,WI) and run in BioRAD thermal cycler. PCR products were run in a 1.5% agarose gel in 1X TBE with SYBRM Safe (10μl/100ml 1.5%agarose; Invitrogen). Gels were imaged using a Chemiluminescent imager (BioRAD). Genotypes were identified with the following primer pair:

VHL F1 (5'-CTG GTA CCC ACG AAA CTG TC-3'), F2 (5'-CTA GGC ACC GAG CTT AGA GGT TTG CG-3'), and R1 (5'-CTG ACT TCA CTG ATG CTT GTC ACA G-3'); Cre F (5'-AGT GCG TTC GAA CGC TAG AGC CTG T-3') and R (5'-GAA CCT GAT GGA CAT GTT CAG G-3'); GCG^{Stopflox} F1 (5'-CCT TCA GAA AAG CTG TCA GA-3'), F2 (5'-GCA TTC TAG TTG TGG TTT GTC C-3'), and RA (5'-TCC TAT GTA ACT GTT TGG CAT G-3'); GLP1R^{Stopflox}-WT F1 (5'- TGA GAG CTG ATG GAA GGT GTT G-3'), Mutant F2 (5'-CTG CAT TCT AGT TGT GGT TTG TCC-3'), and Common R1(5'-CCT TCA GAT GGG GAA ACA AAG C-3'); Hamp F (5-TAG GCT GCT TAC CTC TCT TTC TT-3') and R (5'-AAT TCC AAG ACT TAG AAG GCA AA-3').

Vertical sleeve gastrectomy surgery (VSG)

The day prior to surgery solid food was replaced with liquid diet (Osmolite). Under isoflurane/O₂ mixture anesthesia, all mice received a midline incision in the ventral abdominal wall and the stomach was exposed. For VSG, approximately 80% of the stomach was transected along the greater curvature using an Endopath ETS-FLEX 35mm Stapler (Ethicon endo-surgery) creating a sleeve-like gastric remnant. For sham surgery, pressure was applied on the stomach imitating the VSG-transection line with nontoothed blunt forceps. The abdominal wall was closed using continuous absorbable 5-0 Vicryl Rapide sutures. Postoperatively, mice had ad lib access to Osmolite liquid diet for 4 consecutive days. All mice received 1 ml warm saline subcutaneously for fluid replacement on the first postoperative day and analgesic treatment with meloxicam (0.5 mg/kg) for 3 consecutive days following surgery. Solid diet access was resumed on post-surgery day 4. Body weight and food intake were measured daily for the first week post-surgery. General health status was checked for 10 consecutive days post-surgery.

Glucose tolerance test

During glucose tolerance tests, all mice were fasted for 4 hours prior to intraperitoneal injections of dextrose (2 g/kg body weight). Tail vein blood glucose levels were measured using Accu-Chek glucometers (Accu-Chek) at 0, 15, 30, 45, 60, 90, and 120 minutes post glucose administration. Area under the curve over 120 minutes was calculated.

ELISA

Plasma insulin levels were determined using ELISA colorimetric insulin assay kit (Crystal Chem). For iron measurement, plasma samples were collected from heparinized blood and used for measurement of total circulating iron (Fe²⁺ and Fe³⁺) using the Quanti-Chrom Iron Assay Kit (BioAssay Systems). Plasma hepcidin levels were determined using Hepcidin-Murine Compete™ ELISA (Intrinsic Life Sciences). For GLP-1, whole blood samples were collected in microtubes treated with 1:10 μ l anti-proteolytic cocktail (EDTA/Aprotinin/Heparin) to prevent enzymatic GLP-1 degradation. Plasma total GLP-1 levels were determined using the Meso Scale Discovery Platform according to the manufacturer's instructions (Meso Scale Discovery). All assays were performed according to the manufacturer's instructions.

Luciferase assay

Tissue luciferase activity was measured by homogenizing the tissues of ODD-luciferase reporter mice with the Dual Dual-Luciferase Assay System (Promega) according to the manufacturer's instructions and measured with SpectraMax M5 (Molecular Devices).

Body composition

In vivo lean and adipose tissue body composition in mice and rat was measured using nuclear magnetic resonance (EchoMRI™-900, EchoMRI LLC, Houston, USA).

RT-PCR

To determine mRNA expression from duodenum and ileum, the small intestine was dissected. The duodenum or proximal small intestine was cut from the stomach to app. 3cm in length. The ileum or distal small intestine was cut at app. 5cm proximal to- and at the cecum. Intestinal sections were cut longitudinal and gently rinsed in saline to remove intestinal contents. Tissues were placed on a microscope slide with the epithelial layer facing upwards. Using a clean microscope slide the epithelial layer was scraped from the submucosal layer. The epithelial sample was frozen in liquid nitrogen and stored at -80°C . Epithelial tissue were homogenized using Trizol reagent (Thermo Fisher Scientific). RNA was then extracted using PureLink RNA mini kit (Thermo Fisher Scientific) and cDNA was isolated using iScript cDNA synthesis kit (BioRad). The real-time quantitative PCR was conducted using a CFX-96 Real-Time System (BioRad) with SsoAdvanced Universal Probes Supermix (BioRad) and TaqMan Gene Expression Assays (Thermo Fisher Scientific). Expression levels of target genes were normalized to the average of Rpl32 and Actb gene expressions. Probes used are shown at [key resources table](#).

Transcriptome analysis

Total RNA from the dissected duodenum, jejunum and ileum was isolated using the RNeasy Mini kit including on-column digestion of DNA during RNA purification (Qiagen, Valencia, CA, USA) and was amplified using the Ovation PicoSL WTA System V2 in combination with the Encore Biotin Module (Nugen). Amplified cDNA was hybridized on Rat Gene 2.1 ST arrays (Thermo Fisher Scientific Inc., Waltham, USA). Staining and scanning was done according to the Thermo Fisher Scientific expression protocol including minor modifications as suggested in the Encore Biotin protocol. Expression console (v.1.3.0.187, Thermo Fisher Scientific) was used for quality control and to obtain annotated normalized RNA gene-level data. Statistical analyses were performed by utilizing the statistical programming environment R (R Core Team (2017) *R A Language and Environment for Statistical Computing*,) implemented in CARMA-web (Rainer et al., 2006). Genewise testing for differential expression was done employing the limma t-test and Benjamini-Hochberg multiple testing correction (FDR <10%). Heatmaps were generated with R. Enrichment and upstream regulator analyses were generated through the use of QIAGEN's Ingenuity Pathway Analysis (IPA, QIAGEN Redwood City, www.qiagen.com/ingenuity) using Fisher's Exact Test p-values. Input for the enrichment analyses were regulated genes with FDR<10% in both surgeries and same direction of regulation. For the upstream regulator analysis VSG and RYGB were analyzed separately (FDR<10% and fold-change > 1.3x). Array data have been submitted to the GEO database at NCBI (GSE169403).

QUANTIFICATION AND STATISTICAL ANALYSIS

Statistics

Details of statistical analyses including group sizes (n) are presented in the figure legends. All data are presented as average \pm SEM. All statistical analyses were performed using Graphpad Prism 8.1.2 software (La Jolla, CA). Two groups direct comparisons were performed using t-test. Two groups multiple comparisons were performed using Multiple t-test with Bonferroni correction. Multiple groups with one variable comparison were performed using one-way ANOVA post hoc Tukey. Multiple groups with two variables comparison were performed using two-way ANOVA post hoc Tukey. Multiple group comparisons over time were performed using repeated measures ANOVA post hoc Tukey. Data were considered statistically significant when $P < 0.05$.

Supplemental information

Gut HIF2 α signaling is increased after

VSG, and gut activation of HIF2 α decreases

weight, improves glucose, and increases GLP-1 secretion

Simon S. Evers, Yikai Shao, Sadeesh K. Ramakrishnan, Jae Hoon Shin, Nadejda Bozadjieva-Kramer, Martin Irmeler, Kerstin Stemmer, Darleen A. Sandoval, Yatrik M. Shah, and Randy J. Seeley

Supplement

Figure S1: Body weight progression and composition following RYGB and VSG surgery in rats

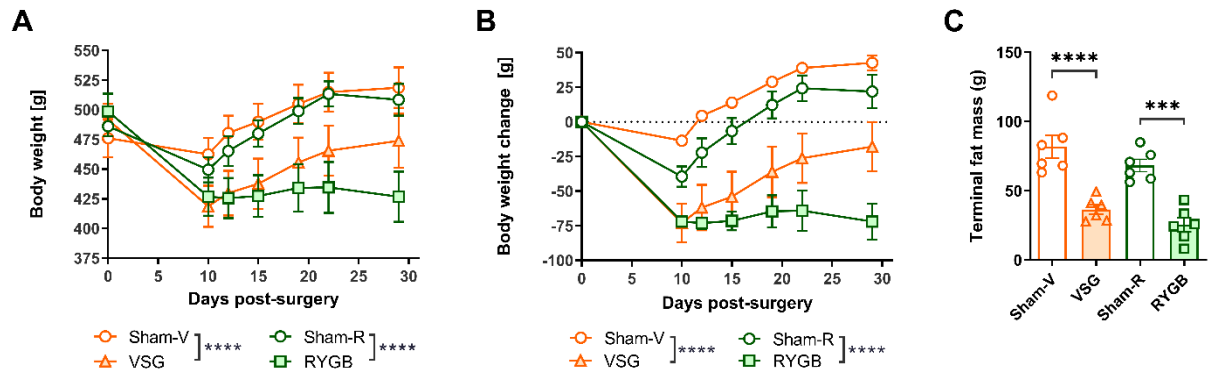


Fig S1) In vivo data from the rat VSG and RYGB cohort used for RNA sequencing analyses of duodenum and ileum. A) Average body weight from time of surgery (day 0) until termination (day 30). Both VSG and RYGB induce weight loss of the course of the study (**** $P < 0.0001$, RM-ANOVA). B) Relative body weight from time of surgery (day 0) until termination (day 30). Both VSG and RYGB induce relative weight loss of the course of the study (**** $P < 0.0001$, RM-ANOVA). C) Fat mass at termination shows both VSG and RYGB result in a reduction of total body adiposity as measured by EchoMRI (*** $P < 0.001$, **** $P < 0.0001$ one-way ANOVA). Data is presented as average \pm sem ($n = 6$ /group). Data is related to methods section: Rat cohort for RNA sequencing study; and manuscript figure 1A-C.

Figure S2: Body weight progression and glucose responses following VSG surgery in high dietary iron fed mice and Hepcidin^{ALIVER} mice.

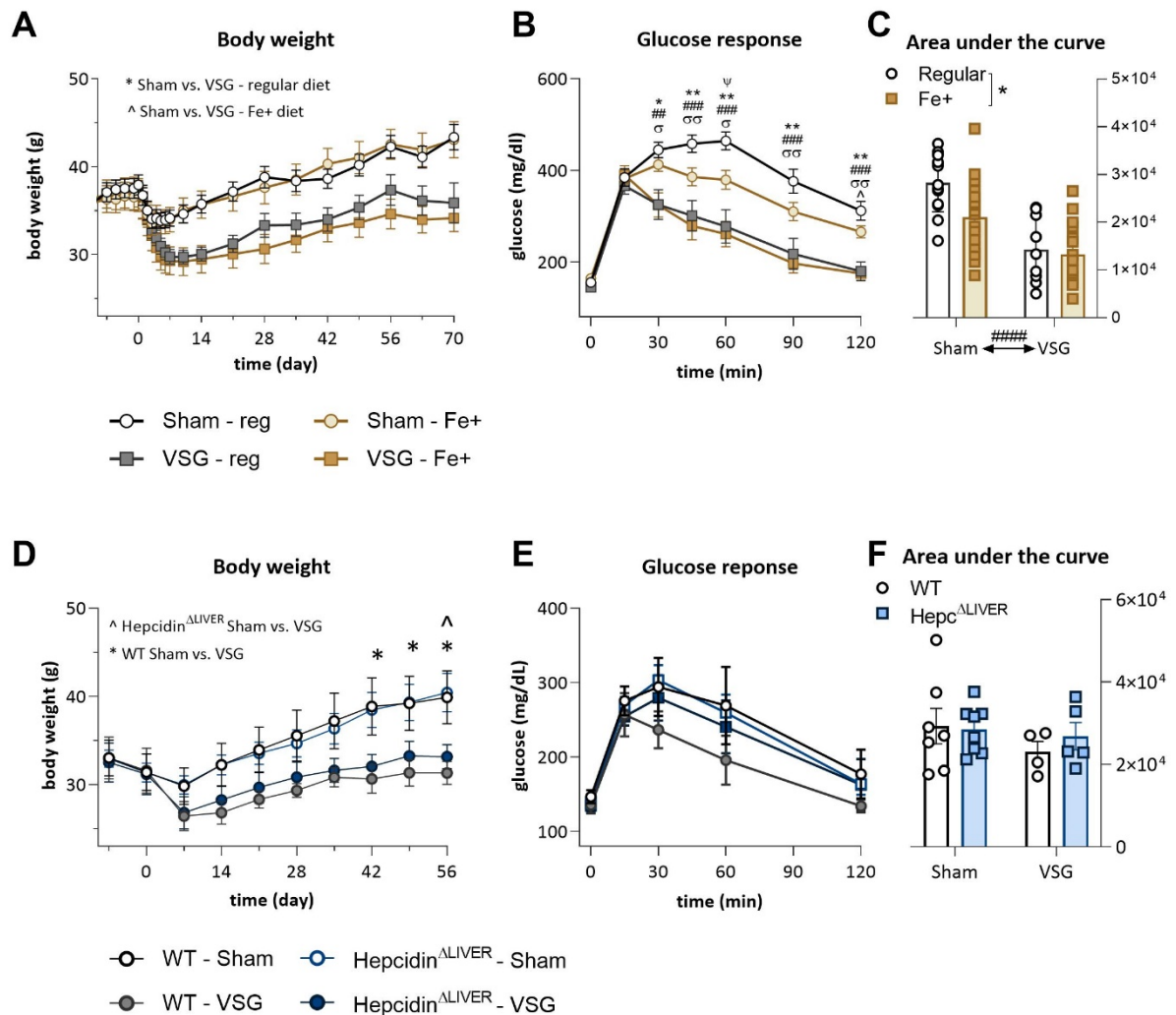


Fig. S2) High dietary iron supplementation or Hepcidin^{ALIVER} do not affect the metabolic response to VSG. A) Mice fed a 45% HFD containing 350ppm supplemented iron responded equally to VSG surgery at the level of body weight maintenance as mice fed a 45% HFD containing 35ppm iron (Two-way ANOVA: $F_{(66, 814)}=13.19$, $P<0.0001$, main effect post hoc Tukey **** $P<0.0001$ Sham-reg>VSG-reg, ##### $P<0.0001$ Sham-reg>VSG-Fe+, ^^^ $P<0.0001$ Sham-Fe+>VSG-reg, $\sigma\sigma\sigma\sigma P<0.001$ Sham-Fe>VSG-Fe+). B) Glucose levels following ip glucose administration (ip 2g/kg glucose) are reduced in VSG compared to Sham groups and lower in Sham-Fe+ compared to Sham-reg (rm-ANOVA: $F_{(18,312)}=6.714$, simple effects per row post hoc Tukey, * $P<0.05$, ** $P<0.01$ Sham-Reg>VSG-reg, ### $P<0.01$, #### $P<0.001$ Sham-reg>VSG-Fe+; $\sigma P<0.05$, $\sigma\sigma P<0.01$ Sham-Fe+>VSG-Fe+, ^ $P<0.05$ Sham-Fe+>VSG-reg; $\psi P<0.05$ Sham-reg>Sham-Fe+). C) The area under the curve of the glucose response is lowered by VSG (Two-way ANOVA, main effects: ##### $P<0.0001$ Surgery effect), but to a lesser extent so did dietary iron ($\sigma P<0.05$ dietary iron effect). Data presented in 2S A-C is related to methods section:

Response to VSG in mice fed a high iron containing diet; and manuscript figure 2A-C. D) Hepcidin^{ΔLiver} mice respond similar to VSG surgery as WT mice at the level of body weight *P<0.05: WT Sham > VSG ^P<0.05: Hepcidin^{ΔLiver} Sham > VSG, post hoc Tukey; E) glucose response, and F) area under the curve of glucose response, E) fasting glucose levels, #P<0.05 two-way ANOVA main effect of surgery. Data is presented as average±sem. Data presented in 2S D-F is related to method section: Response to VSG in a mouse model of hereditary hemochromatosis; and manuscript figure figure 2D-F.

Figure S3: Duodenal mRNA expression in *Hif2α*^{ΔGut} mice following VSG surgery

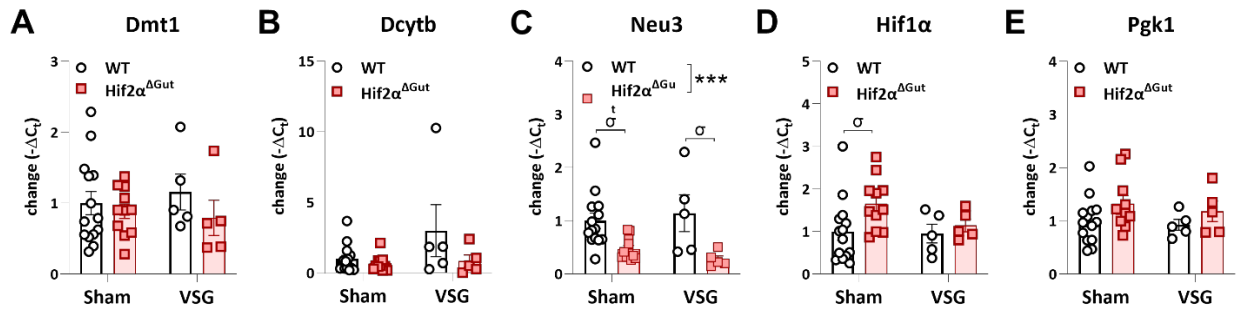


Fig. S3) Non-fasting HIF2 α target genes expressions in duodenal tissue from *Hif2 α ^{ΔGut}* mice that had either sham or VSG surgery show no down regulation of iron transporters A) *Dmt1*, and B) *Dcytb*. C) *Neu3* is down regulated in duodenal tissue of *Hif2 α ^{ΔGut}* mice (***) $P < 0.001$, two-way ANOVA main effect of genotype, $\sigma P < 0.05$ post hoc Tukey. D) An increase of duodenal *Hif1 α* was observed in Sham operated rats ($\sigma P < 0.05$, two-way ANOVA post hoc Tukey). E) No changes in expression of HIF1 α target gene *Pgk1* was observed in duodenal tissue of *Hif2 α ^{ΔGut}* mice independent of surgery. Data is presented as average \pm sem. Data is related to method section: Response to VSG in intestinal *Hif2 α* knockout mice; and manuscript figure 3. Average Ct data are presented in Table S4.

Supplemental Tables:

Table S1: Cycle threshold (Ct) of gene expression in the duodenum and ileum.

Gene of interest:	Vhl		Phd2		Hif2a		Dmt1		Dcytb		Neu3		Hif1a		Pgk1		Glut1	
	Avg	sem	Avg	sem	Avg	sem	Avg	sem	Avg	sem	Avg	sem	Avg	sem	Avg	sem	Avg	sem
Duodenum (Ct, n=8)	32.33	0.24	29.35	0.25	28.84	0.26	27.76	0.24	30.18	0.30	33.66	0.37	28.36	0.25	26.50	0.27	32.65	0.33
Ileum (Ct, n=8)	31.90	0.16	29.06	0.16	30.32	0.16	29.18	0.18	35.55	0.35	37.07	0.23	28.98	0.21	26.57	0.18	32.33	0.30

Numbers are presented as average (Avg) \pm standard error of the mean (sem) referring to Δ Ct gene expression levels in figure 1F.

Table S2: Cycle threshold (Ct) of gene expression in the duodenum of VSG and Sham operated mice.

Gene of interest:	Vhl		Phd2		Hif2a		Dmt1		Dcytb		Neu3		Hif1a		Pgk1		Glut1	
	Avg	sem	Avg	sem	Avg	sem	Avg	sem	Avg	sem	Avg	sem	Avg	sem	Avg	sem	Avg	sem
VSG (Ct, n=16)	32.03	0.09	28.75	0.13	28.97	0.10	27.68	0.20	29.50	0.29	33.70	0.15	27.73	0.17	25.50	0.15	32.24	0.20
Sham (Ct, n=8)	32.33	0.41	29.08	0.45	28.82	0.29	28.52	0.41	31.10	0.64	34.14	0.40	27.61	0.36	25.74	0.44	32.58	0.35

Numbers are presented as average (Avg) \pm standard error of the mean (sem) referring to Δ Ct gene expression levels in figure 1G.

Table S3: Cycle threshold (Ct) of gene expression in the duodenum of WT and Hif2 $\alpha^{\Delta\text{Gut}}$ mice.

Gene of interest: Surgery group:	Hif2a-Exon2-3				Cre			
	Sham		VSG		Sham		VSG	
	<i>Avg</i>	<i>sem</i>	<i>Avg</i>	<i>sem</i>	<i>Avg</i>	<i>sem</i>	<i>Avg</i>	<i>sem</i>
WT	31.59	1.06	32.28	1.38	39.63	2.69	43.82	2.89
Hif2$\alpha^{\Delta\text{Gut}}$	34.74	0.30	35.16	1.01	30.47	0.21	30.28	0.49

Groups sizes: Wt-Sham: n=14, Wt-VSG: n=6, Hif $\alpha^{\Delta\text{Gut}}$ -Sham: n=13, Hif $\alpha^{\Delta\text{Gut}}$ -VSG: n=6.

Numbers are presented as average (Avg) \pm standard error of the mean (sem) referring to ΔCt gene expression levels in figure 3A/B.

Table S4: Cycle threshold (Ct) of gene expression in the duodenum of WT and Hif2 $\alpha^{\Delta\text{Gut}}$ mice.

Gene of interest: Surgery group:	Dmt1				Dcytb				Neu3				Hif1a				Pkg1			
	Sham		VSG		Sham		VSG		Sham		VSG		Sham		VSG		Sham		VSG	
	<i>Avg</i>	<i>sem</i>	<i>Avg</i>	<i>sem</i>	<i>Avg</i>	<i>sem</i>	<i>Avg</i>	<i>sem</i>	<i>Avg</i>	<i>sem</i>	<i>Avg</i>	<i>sem</i>	<i>Avg</i>	<i>sem</i>	<i>Avg</i>	<i>sem</i>	<i>Avg</i>	<i>sem</i>	<i>Avg</i>	<i>sem</i>
WT	32.09	1.15	32.21	1.80	36.36	1.41	35.51	2.67	35.27	1.16	35.91	1.33	30.63	1.42	31.26	1.37	30.12	0.94	30.66	0.79
Hif2$\alpha^{\Delta\text{Gut}}$	32.43	0.34	32.00	1.25	36.77	0.24	36.73	2.37	36.29	0.21	36.80	0.90	29.87	0.32	29.85	0.69	29.78	0.18	29.55	0.63

Groups sizes: Wt-Sham: n=14, Wt-VSG: n=6, Hif $\alpha^{\Delta\text{Gut}}$ -Sham: n=13, Hif $\alpha^{\Delta\text{Gut}}$ -VSG: n=6..

Numbers are presented as average (Avg) \pm standard error of the mean (sem) referring to ΔCt gene expression levels in supplement figure S3.

Table S5: Cycle threshold (Ct) of gene expression in the duodenum of WT and Vhl^{ΔGut} mice.

Gene of interest:	Vhl		Phd2		Hif2a		Dmt1		Dcytb		Neu3		Hif1a		Glut1		Pgk1		Pdk1	
	Avg	sem	Avg	sem	Avg	sem	Avg	sem	Avg	sem	Avg	sem	Avg	sem	Avg	sem	Avg	sem	Avg	sem
WT (Ct, n=8)	33.60	0.20	31.57	0.20	29.93	0.22	28.91	0.38	32.52	0.61	34.88	0.48	29.79	0.19	34.47	0.32	28.40	0.30	32.94	0.23
Vhl^{ΔGut} (Ct, n=8)	NA	NA	28.86	0.28	29.25	0.18	25.49	0.30	25.71	0.29	29.41	0.24	32.46	0.24	32.67	0.38	27.35	0.32	30.89	0.30

Numbers are presented as average (Avg) ± standard error of the mean (sem) referring to ΔCt gene expression levels in figure 4A.

Table S6: Cycle threshold (Ct) of gene expression in the ileum of WT and Vhl^{ΔGut} mice.

Gene of interest:	Vhl		Phd2		Hif2a		Dmt1		Dcytb		Neu3		Hif1a		Glut1		Pgk1		Pdk1	
	Avg	sem	Avg	sem	Avg	sem	Avg	sem	Avg	sem	Avg	sem	Avg	sem	Avg	sem	Avg	sem	Avg	sem
WT (Ct, n=8)	32.50	0.20	28.98	0.20	29.89	0.30	29.19	0.22	37.19	0.36	36.94	0.14	28.10	0.23	31.49	0.26	25.53	0.23	30.83	0.19
Vhl^{ΔGut} (Ct, n=8)	NA	NA	27.56	0.25	29.53	0.10	25.52	0.21	33.52	0.38	35.99	0.22	29.41	0.28	29.85	0.26	23.87	0.38	27.56	0.25

Numbers are presented as average (Avg) ± standard error of the mean (sem) referring to ΔCt gene expression levels in figure 4B.

Table S7: Oligonucleotides section of Key Resource Table

REAGENT or RESOURCE	SOURCE	IDENTIFIER
Oligonucleotides		
<i>Vhl</i> - F1 (5'-CTG GTA CCC ACG AAA CTG TC-3')	Integrated DNA technologies	N/A
<i>Vhl</i> - F2 (5'-CTA GGC ACC GAG CTT AGA GGT TTG CG-3')	Integrated DNA technologies	N/A
<i>Vhl</i> - R1 (5'-CTG ACT TCA CTG ATG CTT GTC ACA G-3')	Integrated DNA technologies	N/A
<i>Cre</i> - F (5'-AGT GCG TTC GAA CGC TAG AGC CTG T-3')	Integrated DNA technologies	N/A
<i>Cre</i> - R (5'-GAA CCT GAT GGA CAT GTT CAG G-3')	Integrated DNA technologies	N/A
<i>Gcg</i> - F1 (5'-CCT TCA GAA AAG CTG TCA GA-3')	Integrated DNA technologies	N/A
<i>Gcg</i> - F2 (5'-GCA TTC TAG TTG TGG TTT GTC C-3')	Integrated DNA technologies	N/A
<i>Gcg</i> - RA (5'-TCC TAT GTA ACT GTT TGG CAT G-3')	Integrated DNA technologies	N/A
<i>Glp1r</i> - F1 (5'- TGA GAG CTG ATG GAA GGT GTT G-3')	Integrated DNA technologies	N/A
<i>Glp1r</i> - Mutant F2 (5'-CTG CAT TCT AGT TGT GGT TTG TCC-3')	Integrated DNA technologies	N/A
<i>Glp1r</i> - Common R1(5'-CCT TCA GAT GGG GAA ACA AAG C-3')	Integrated DNA technologies	N/A
<i>Hamp</i> - F (5'-TAG GCT GCT TAC CTC TCT TTC TT-3')	Integrated DNA technologies	N/A
<i>Hamp</i> - R (5'-AAT TCC AAG ACT TAG AAG GCA AA-3')	Integrated DNA technologies	N/A

This table is related to the Key Resource Table in the STAR methods section of the manuscript.